



NATIONAL ADVISORY COMMITTEE FOR AERONAUTICS

TECHNICAL NOTE 4146

CONTRIBUTION OF THE WING PANELS TO THE FORCES
AND MOMENTS OF SUPERSONIC WING-BODY
COMBINATIONS AT COMBINED ANGLES

By J. Richard Spahr

Ames Aeronautical Laboratory
Moffett Field, Calif.



Washington
January 1958

AFMCG
TECHNICAL LIBRARY
APR 20 1958

10483 89401
NACA TN 4146



NATIONAL ADVISORY COMMITTEE FOR AERONAUTICS

TECHNICAL NOTE 4146

CONTRIBUTION OF THE WING PANELS TO THE FORCES
AND MOMENTS OF SUPERSONIC WING-BODY
COMBINATIONS AT COMBINED ANGLES

By J. Richard Spahr

SUMMARY

A wind-tunnel investigation was conducted at a Mach number of 1.96 and at Reynolds numbers (based on the mean aerodynamic chord of the exposed wing) of 0.36 and 1.03 million to determine the normal forces, pitching moments, and rolling moments contributed by each wing panel of a cruciform-wing and body combination over a wide range of combined angles of pitch and roll. The wings were triangular of aspect ratio 2, and the body was an ogive-cylinder combination. The effects of forebody length and roughness and of the presence of the adjacent panels on these panel contributions were determined.

The results of the investigation show that large changes in the panel forces and moments can occur as the result of combined angles. A general theoretical method based on slender-body and strip theories was found to yield results in good agreement with the wind-tunnel measurements. These comparisons indicate that the changes in the panel characteristics due to combined angles are caused primarily by a cross coupling between the side-wash velocities due to angle of attack and sideslip and by the presence of forebody vortices due to crossflow separation. It was found that an increase in forebody length increases the effect of the forebody vortices because of the dependence of the strength of these vortices on the forebody length.

An application of these panel results to wing-body combinations shows that the effects of combined angles have only a small influence on the forces and moments of a cruciform-wing and body combination. However, for a planar-wing and body combination these effects cause a loss in the normal force, a negative pitching-moment increment, and an increase in the magnitude of the rolling moment when the sideslip angle is increased. The results for a tail-body combination indicate that the effects of combined angles of attack and sideslip have only a small influence on the longitudinal or directional stability contribution of either a "+" or "X" tail arrangement, but these effects cause a serious loss with increasing angle of attack in the directional stability of a conventional tail

arrangement having an upper vertical fin. If this fin is replaced by a lower (ventral) fin, an increase in the directional stability with angle of attack occurs. The results also show that either a "V" or an "inverted V" tail arrangement provides a contribution to the directional stability of a tail-body combination which is nearly independent of angle of attack, but such tails exhibit undesirable longitudinal trim changes with sideslip.

INTRODUCTION

With the trend toward higher Mach numbers and altitudes, airplanes and missiles are required to operate over wider ranges of angles of attack and sideslip. A number of static-stability problems are encountered under these conditions for which present aerodynamic theory is inadequate. Among the more important of these problems are:

- (a) Deterioration in directional stability with increasing angle of attack.
- (b) Nonlinear variation of yawing moment with angle of sideslip at large angles of attack.
- (c) Change in pitching moment due to sideslip at large angles of attack.
- (d) Variation of dihedral effect (rolling moment due to sideslip) with angle of attack or induced rolling moments at combined angles of pitch and roll.
- (e) Panel-panel interference for multipanel wing or tail arrangements.

These problems stem largely from the contributions of the individual wing and tail panels to the forces and moments on complete combinations. However, no systematic experimental results or general theoretical methods are available to provide an adequate understanding of the aerodynamic characteristics of wing or tail panels in the presence of a body at combined angles of attack and sideslip.

The purpose of the present investigation, therefore, was to investigate the contributions of each wing panel to the normal forces, pitching moments, and rolling moments of various wing-body combinations through a wide range of combined angles of pitch and roll and to develop a general calculative method for predicting these panel characteristics. The effects of forebody length and roughness, Reynolds number, and panel-panel interference were investigated. The panel results are applied to a comparison of the contribution of the wing or tail surfaces in various arrangements to the aerodynamic forces and moments of several wing-body and tail-body combinations.

NOTATION

a	body radius
b	maximum span of wing-body combination
C_l	rolling-moment coefficient, $\frac{\text{rolling moment about X axis}}{qS_l}$ (See fig. 1.)
C_m	pitching-moment coefficient, $\frac{\text{pitching moment about Y axis}}{qS\bar{c}}$ (See figs. 1 and 2(a).)
C_m'	pitching-moment coefficient, $\frac{\text{pitching moment about } Y_t \text{ axis}}{qS\bar{c}}$ (See figs. 1 and 2(a).)
C_N	normal-force coefficient, $\frac{\text{force in the Z direction}}{qS}$ (See fig. 1.)
C_N'	normal-force coefficient, $\frac{\text{force in the } Z_t \text{ direction}}{qS}$ (See fig. 1.)
C_{N_α}	$\frac{dC_N}{d\alpha}$
C_n	yawing-moment coefficient, $\frac{\text{yawing moment about Z axis}}{qS\bar{c}}$ (See fig. 1(b).)
C_Y	side-force coefficient, $\frac{\text{force in the Y direction}}{qS}$ (See fig. 1(b).)
C_{Y_β}	$\frac{dC_Y}{d\beta}$
c	local chord of panel
\bar{c}	mean aerodynamic chord of exposed panel, $\frac{\int_a^{s_m} c^2 dy}{\int_a^{s_m} c dy}$

c_o	panel chord at body center line
c_r	panel chord at wing-body juncture
c_t	panel chord at tip
E	elliptic integral of the second kind
F	incomplete elliptic integral of the first kind
K	complete elliptic integral of the first kind
K_w	ratio of lift on a wing in the presence of a body to lift on the wing alone
K_ϕ	factor representing the coupling between the sidewash velocities due to α and β
l	reference length (s_m for single-panel results and b for multipanel results)
Δp	difference in static pressure between lower and upper surface of panel
q	free-stream dynamic pressure, $\frac{1}{2}\rho V^2$
R	Reynolds number based on \bar{c}
S	reference area (exposed plan-form area of one panel for single-panel results and area of two panels for multipanel results)
s_m	maximum semispan of wing-body combination, $\frac{b}{2}$
V	free-stream velocity
w	fluid velocity component in Z direction
x, y, z	Cartesian coordinates fixed in the body (See fig. 1(a).)
x_t, y_t, z_t	Cartesian coordinates obtained by rotating the x, y, z system through an angle ϕ about the X axis (See fig. 1(a).)
x_{cp}	distance along X axis from the leading edge of the panel root chord (at body juncture) to the center of pressure of the loading on the panel

y_{cp}	distance along Y axis from the origin to the center of pressure of the loading on the panel
y_v, z_v	coordinates in the Y-Z plane of the location of a vortex
α	angle of attack (See fig. 1(b).)
β	angle of sideslip (See fig. 1(b).)
Γ	circulation
ϵ	semiapex angle of wing plan form
θ	angle of pitch (See fig. 1(a).)
Λ	sweepback angle of panel leading edge
λ	taper ratio of panel, $\frac{c_t}{c_o}$
ρ	free-stream fluid mass density
ϕ	angle of roll (See fig. 1(a).)

Subscripts

1	right-hand horizontal panel (viewed from the rear)
2	lower vertical panel
3	left-hand horizontal panel (viewed from the rear)
4	upper vertical panel
w	wing alone
α	quantity due to angle of attack or sideslip
ϕ	quantity due to effects of combined angles of attack and sideslip or quantity at an angle of roll

Configuration Designations

B_S short forebody (See fig. 2(a).)

B_L long forebody (See fig. 2(a).)

$\left. \begin{matrix} W_1, W_2 \\ W_3, W_4 \end{matrix} \right\}$ wing panels (See fig. 1.)

The configuration is identified first by the wing panel(s) for which results are presented, followed in parentheses by the remaining components present. Thus, for example $W_1W_3(B_LW_4)$ signifies force and moment data for wing panels W_1 and W_3 in the presence of B_LW_4 .

APPARATUS

Wind Tunnel

The Ames 1- by 3-foot supersonic wind tunnel No. 1, in which the investigation was conducted, is a closed-circuit continuous-operation wind tunnel having independently variable Mach number and Reynolds number. The Mach number is varied by adjusting the flexible plates which comprise the upper and lower walls of the nozzle, and the Reynolds number is varied by changing the stagnation pressure in the wind tunnel. The Mach number range of the wind tunnel at the time of the present tests was 1.2 to 2.5 but since that time the upper limit has been increased to 4.0.

Model and Support

The model consisted of a cruciform wing in combination with a cylindrical body of revolution having an ogival nose as shown in figure 2. The model was provided with two alternate forebodies (portion forward of the wing) having identical nose sections but of different length. Geometric characteristics of the configuration are listed in table I. Wing panel W_1 was supported by a two-component strain-gage balance mounted inside the body for measuring the normal force and pitching moment acting on the panel. An additional strain gage was mounted on the surface of the wing panel just inside the body for measuring the rolling moment acting on the panel. A small gap (approximately 0.003 inch) between the wing root and the body prevented the transfer of any portion of the wing panel load to the body without first passing through the strain-gage system. The other three panels were attached directly to the body.

The body was mounted on an unshrouded sting as shown in figure 2(b) which was connected to a remotely controlled motorized mechanism which enabled the model to be rotated about its axis to any roll angle. This mechanism was mounted on a support having its center of rotation coincident with the transverse center line of the wind-tunnel test section to provide an angle-of-pitch range of $\pm 18^\circ$. In order to increase this range in the positive direction, the model and roll mechanism were set at a pitch angle of 15° relative to the pitch support, thereby changing the angle-of-pitch range to -3° to 33° .

TESTS AND PROCEDURE

Test Conditions

Tests were conducted at a Mach number of 1.96 through a nominal angle-of-pitch range of -3° to 33° for several constant angles of roll from -90° to 90° and at Reynolds numbers of 0.36 and 1.03×10^6 , based on the wing-panel mean aerodynamic chord. Forces and moments on panel W_1 were measured for each of the configurations listed in the following table.

Configuration	Long forebody, B_L		Short forebody, B_S	
	$R = 0.36 \times 10^6$	$R = 1.03 \times 10^6$	$R = 0.36 \times 10^6$	$R = 1.03 \times 10^6$
$W_1(B)$	X	X	X	X
$W_1(BW_2)$		X	X	X
$W_1(BW_3)$		X		X
$W_1(BW_4)$		X	X	X
$W_1(BW_2W_3)$		X		X
$W_1(BW_2W_4)$		X	X	X
$W_1(BW_3W_4)$		X		X
$W_1(BW_2W_3W_4)$		X		X
$W_1(B)$ with roughness	X	X		X

The roughness denoted for the final configuration consisted of a uniform layer of salt crystals on all but the most rearward portion ($3/4$ in.) of the forebody.

Precision of Data

The uncertainties in the panel force and moment data and in the independent quantities have been calculated from the precision of the contributing measurements. Representative values of these estimated uncertainties are listed in the following table.

Quantity	Uncertainty	
	$\theta = 0^\circ$	$\theta = 25^\circ$
C_N	± 0.002	± 0.007
C_m	± 0.001	± 0.004
C_L	± 0.001	± 0.003
θ	$\pm 0.05^\circ$	
ϕ	$\pm 0.40^\circ$	
M	± 0.015	
R	$\pm 0.006 \times 10^8$	

As a check of the precision, approximately one-fifth of the tests were rerun. The repeatability of the data from these runs was in essential agreement with the estimated uncertainties given in the preceding table.

An estimate was made of the effects on the data of the nonuniformities in the wind-tunnel stream. These effects were within the precision of the results and thus no corrections were made.

THEORETICAL METHOD

Existing theoretical methods, such as the one given in reference 1, for the calculation of the forces and moments on a lifting surface in the presence of a body are restricted to low or moderate angles of attack and to zero sideslip. The purpose of the present theoretical study is to develop a general calculative method for the prediction of these panel characteristics over a wide range of combined angles of attack and sideslip. The fundamental basis of this method is the assumption that the loading on a wing or tail panel in the presence of a body at an arbitrary angle of attack and sideslip is equal to the sum of the loading due to potential flow (no separation) and that due to viscous separation effects of the forebody crossflow. The development of a general method for the calculation of these two components of the panel loads is discussed in the succeeding paragraphs.

Potential Flow

The theory of reference 2 for slender wing-body combinations was employed in reference 1 to develop expressions for calculating the normal force and pitching moment on the wing panels of nonslender as well as slender wing-body combinations having cylindrical bodies at angle of

attack and zero sideslip. These expressions are extended in Appendix A of the present report to apply to the general case of combined angles of attack and sideslip by integrating the equations (derived in ref. 3) for the load distribution on slender wing panels in the presence of a body at combined angles. In addition, expressions are derived for the rolling moment contributed by the wing panels. Equations are presented in Appendix A for the normal force or side force, pitching or yawing moment, and rolling moment on each wing panel of a planar or cruciform wing-body combination. Typical of these equations are those for the right horizontal panel (W_1 in fig. 1):

$$C_N = C_{N_{\alpha, w(\beta=0)}} \left(K_w \alpha + \frac{K_\phi}{\tan \epsilon} \alpha \beta \right) \quad (1)$$

$$C_m = -C_{N_{\alpha, w(\beta=0)}} \left[K_w \left(\frac{x_{cp}}{\bar{c}} \right)_\alpha \alpha + \frac{K_\phi}{\tan \epsilon} \left(\frac{x_{cp}}{\bar{c}} \right)_\phi \alpha \beta \right] \quad (2)$$

$$C_l = -C_{N_{\alpha, w(\beta=0)}} \left[K_w \left(\frac{y_{cp}}{s_m} \right)_\alpha + \frac{K_\phi}{\tan \epsilon} \left(\frac{y_{cp}}{s_m} \right)_\phi \alpha \beta \right] \quad (3)$$

or in terms of angles of pitch θ and roll ϕ

$$C_N = C_{N_{\theta, w(\phi=0)}} \left(K_w \theta \cos \phi + \frac{K_\phi}{\tan \epsilon} \theta^2 \sin \phi \cos \phi \right) \quad (4)$$

$$C_m = -C_{N_{\theta, w(\phi=0)}} \left[K_w \left(\frac{x_{cp}}{\bar{c}} \right)_\alpha \theta \cos \phi + \frac{K_\phi}{\tan \epsilon} \left(\frac{x_{cp}}{\bar{c}} \right)_\phi \theta^2 \sin \phi \cos \phi \right] \quad (5)$$

$$C_l = -C_{N_{\theta, w(\phi=0)}} \left[K_w \left(\frac{y_{cp}}{s_m} \right)_\alpha \theta \cos \phi + \frac{K_\phi}{\tan \epsilon} \left(\frac{y_{cp}}{s_m} \right)_\phi \theta^2 \sin \phi \cos \phi \right] \quad (6)$$

since

$$C_{N_{\alpha, w(\beta=0)}} = C_{N_{\theta, w(\phi=0)}}$$

$$\alpha = \theta \cos \phi$$

$$\beta = \theta \sin \phi$$

The first term in each of these equations represents the force or moment due to angle of attack, and the second term represents the additional force or moment due to combined angles resulting from a cross coupling of the sidewash velocities associated with angle of attack and with angle of sideslip. The factors K_w , K_ϕ , $(y_{cp})_\alpha$, and $(y_{cp})_\phi$ depend only on the ratio of the body radius to the panel semispan a/s_m , and values of these quantities can be obtained from the curves of figure 3. The quantities $(x_{cp})_\alpha$ and $(x_{cp})_\phi$, however, depend upon the plan-form shape, and the curves given in figure 3 for these quantities have been computed for triangular plan forms. The effects of panel-panel interference on the panel characteristics in roll are shown in figure 3(b) by a comparison of the planar and cruciform configurations. The differences between these two cases are caused by the presence of the vertical panels. Since the panel loading represented by K_ϕ is the result of a cross coupling between the sidewash velocities due to angle of attack and sideslip, the vertical panels inhibit this coupling, causing a reduction in K_ϕ . This interference becomes smaller as a/s_m increases because the vertical panels effectively move away from the region of influence of the flow field over the horizontal panels.

In all the formulas for the forces and moments on the wing panels (eqs. (A7) to (A18)) the normal-force or side-force curve slope $C_{N_{\alpha,w}(\beta=0)}$ or $C_{Y_{\beta,w}(\alpha=0)}$ of the wing alone is a factor. This implies that the normal-force coefficient of the wing C_{N_w} is a linear function of its angle of attack. It is known from experiment, however, that this linearity is limited to small or moderate angles. Thus, in the practical application of the equations beyond the linear range, more realistic values of C_{N_w} should be used for the product $C_{N_{\alpha,w}}\alpha$, as given by experiment, empirical relationships, or nonlinear theory. The experimental wing results used in these equations for the present investigation are presented in table II. These values of normal force were measured on one wing panel mounted on a boundary-layer plate which served both as a flow reflection plane and as a means of placing the wing in a region free of the tunnel-wall boundary layer.

Effects of Forebody Vortices

At moderate and large angles of inclination the flow over a body is characterized by a pair of symmetrically disposed vortices on the leeward side caused by crossflow separation. When these vortices pass in the vicinity of a lifting surface, such as a wing panel, the loading on the surface is changed by virtue of the induced flow field created by the vortices, and thus the panel forces and moments are changed. The evaluation of these effects requires knowledge of the strength and positions of

the vortices discharged from the body. In reference 4 it was demonstrated that the strength and paths of these vortices can be calculated satisfactorily by means of a stepwise procedure based on incompressible vortex theory, provided the most forward positions at which the vortices are discharged from the body are known. Thus, the experimental determination of the vortex origin is required before the properties of the body vortices can be calculated. For the calculations of the present report, the results of reference 4 for the strength and positions of the vortices were used, since identical bodies at the same Mach number were employed in both investigations.

The calculation of the effects of the body vortices on the wing-panel loading is made most simply by strip theory. It is assumed that the strength and path of each vortex remain unchanged by the addition of the wing panel to the body. Thus, the panel forces and moments due to each vortex are proportional to the integral over the panel surface of the product of the local chord and the local downwash induced by a two-dimensional incompressible vortex. The total forces and moments caused by the body vortex system are given by the sum of the contributions of the two external vortices and their images. General analytical expressions are derived in Appendix B for the normal force, pitching moment, and rolling moment on a wing panel due to any number of vortices of known strength and position. The only restrictions on the wing-body combination are that the wing plan form have straight edges, the body be a circular cylinder, and the wing panels lie in a meridian plane of the body.

RESULTS AND DISCUSSION

Individual Panels

The basic experimental results are presented in figure 4 in which the variation in the normal-force, pitching-moment, and rolling-moment coefficients of panel W_1 are plotted as functions of the pitch angle θ for angles of roll ϕ from -90° to 90° . Results are shown for the characteristics of this panel in the presence of the body alone and with all possible combinations of the other three panels, as identified by the sketches on each part of the figure. On the left-hand side of each page are shown the results for the long forebody B_L and on the right-hand side, the results for the short forebody B_S . Although the results of figure 4 apply only to panel W_1 , the characteristics of the other panels can be obtained from these results by means of the following relationships, which are derived from symmetry considerations:

$$\left. \begin{aligned} (C_{N_2})_{\varphi} &= (C_{N_1})_{90^\circ - \varphi} \\ (C_{N_3})_{\varphi} &= (C_{N_1})_{-\varphi} \\ (C_{N_4})_{\varphi} &= (C_{N_1})_{\varphi - 90^\circ} \end{aligned} \right\} \quad (7)$$

$$\left. \begin{aligned} (C_{m_2})_{\varphi} &= (C_{m_1})_{90^\circ - \varphi} \\ (C_{m_3})_{\varphi} &= (C_{m_1})_{-\varphi} \\ (C_{m_4})_{\varphi} &= (C_{m_1})_{\varphi - 90^\circ} \end{aligned} \right\} \quad (8)$$

$$\left. \begin{aligned} (C_{l_2})_{\varphi} &= -(C_{l_1})_{90^\circ - \varphi} \\ (C_{l_3})_{\varphi} &= -(C_{l_1})_{-\varphi} \\ (C_{l_4})_{\varphi} &= (C_{l_1})_{\varphi - 90^\circ} \end{aligned} \right\} \quad (9)$$

Figure 4 shows that all of the panel characteristics become less symmetrical with roll angle as the angle of pitch is increased. It is seen that at increasing positive roll angles, where the panel is on the windward side of the body, the variations with angle of pitch become more nearly linear. At negative roll angles, however, where the panel is on the leeward side of the body, large losses in the forces and moments occur at high angles of pitch, and these losses reach a maximum at a roll angle of -67.5° . It is noted that as the angle of pitch is increased the maximum normal force and rolling moment occur not at a roll angle of zero but at an increasing positive roll angle.

The influence of roll angle on the panel characteristics at high angles of pitch, as indicated in figure 4, is the result of two different effects. First, a cross coupling occurs between the sidewash velocities due to the components of the crossflow normal and parallel to the wing panel. As a result, the lift effectiveness of the panel increases with positive roll angles and decreases with negative angles. Second, the two vortices due to the forebody crossflow separation tend to reduce the panel normal force at large angles of pitch. This reduction is diminished at positive angles of roll and reaches a maximum at negative angles where the panel is close to one of the vortices.

A comparison is presented in figure 5 of some representative experimental panel results from figure 4 with the results computed by the present theoretical method. On the left-hand side of the figure are shown the variations of normal force, pitching moment, and rolling moment of the wing panel with angle of pitch for zero angle of roll, and on the right are shown the variations of these quantities with roll angle at a pitch angle of 20° . Three theoretical curves are shown to illustrate the contribution of the aerodynamic effects involved: first, the low angle theory, given by the first terms in equations (4), (5), and (6); second, the theory including the cross-coupling effects, given by both terms in these equations; and third, the theory including both the cross coupling and vortex effects. It can be seen from these comparisons that a reasonably close approximation to the experimental wing-panel results is obtained through the use of the present method if these two effects are included. The remaining differences between the calculated and experimental results are an indication of the influence of the additional effects neglected in the method. These effects include differences in dynamic pressure between the windward and leeward wing panels, higher order angle-of-attack and -sideslip effects, and the influence of the wing panel on the forebody-vortex paths. It has been estimated, however, that for the angles and configuration of the present investigation these effects are small in comparison with those considered in the calculative method. The results of figure 5 also indicate that the vortex effects are small or negligible at low angles of pitch or at large positive angles of roll. This result, of course, stems from the fact that at small angles of pitch the body vortices are weak, and at positive angles of roll the wing panel is a large distance away from the body vortices. This latter effect can be seen more clearly by referring to figure 6. In this figure, the contribution of both vortices and their images are shown for the same conditions as those of figure 5(b). It is noted that the net normal force, pitching moment, and rolling moment contributed by the vortices approach 0 as the angle of roll increases to 90° because the effects of the vortices on the right side of the body are equal and opposite to those on the left side. The panel experiences an additional positive normal force from vortices 1 and 3 because the panel is operating in an upwash field from these two vortices, whereas the panel incurs a negative normal-force contribution from vortices 2 and 4 because it is operating in a downwash field from these vortices. As the panel is rotated through a negative angle of roll to the upper side of the body, increasing net forces and moments are induced on the panel by the vortex system. It can be seen that these net forces and moments originate primarily from vortex 1. The predominance of vortex 1 is caused by the fact that the wing panel passes through this vortex, and thus incurs the greatest change in loading. The point of coincidence between this vortex and the wing panel is indicated by the roll angle of approximately -70° , where the forces and moments due to the vortices are a maximum.

Forebody length. - The effects of forebody length on the forces and moments of the wing panel are shown in figure 7 for two angles of pitch, 10° and 25° . It is observed from these results that the principal effect

of reducing the forebody length is to change the panel characteristics at negative angles of roll. This reduction is associated with a reduction in the forebody vortex strength; that is, with the short forebody, there is less reduction in the normal force, pitching moment, and rolling moment at angles of roll near -70° . The center of pressure, calculated from these results, moves rearward and outboard with increasing negative angles of roll. This movement increases with angle of pitch and with nose length. This center-of-pressure change, which is associated with vortex 1, is caused by the increased load on the panel tip and the decreased load near the root associated with the downwash distribution from this vortex; hence, an outboard shift in the center of pressure occurs and for a sweptback plan form this outboard shift is accompanied by a rearward shift. These effects of forebody length can be predicted satisfactorily from the known initial vortex positions through the use of the theoretical method described previously.

Reynolds number and body roughness.- Typical results are shown in figure 8 for two different Reynolds numbers at two angles of pitch, and for the forebody smooth and with roughness added. The purpose of these changes was to investigate the influence of changes in Reynolds number and roughness on the nature of the forebody crossflow vortices by means of their effects on the panel forces and moments. It can be seen from these results that neither change had any effect on the forces or moments acting on the panel under these conditions.

Wing-panel-panel interference.- The effects of the presence of adjacent surfaces on the forces or moments acting on panel W_1 are presented in figure 9. The results for the long forebody are shown in figure 9(a) and those for the short forebody in figure 9(b). It can be seen that, in general, the panel-panel interference is small or negligible at an angle of pitch of 10° in both cases. However, at an angle of 25° , the normal force and rolling moment of the wing panel are influenced by panel-panel interference. It can be observed that the addition of panel 3 or 4 has no influence on the loads on panel 1. However, when panel 2 is added an increase in the normal force and rolling moment occurs at positive angles of roll, and a decrease in these characteristics occurs at negative angles. It can be shown from theoretical considerations that panel-panel interference is associated partly with the cross coupling of the sidewash velocities in potential flow and partly with interference effects of the forebody vortex flow.

Panel Combinations

The characteristics of individual panels just considered can be used to study the characteristics of panel combinations of practical interest, such as wings and tails of complete configurations, through the use of equations (7), (8), and (9). In the following discussion, the contribution

of planar and cruciform wings to the forces and moments on wing-body combinations will first be examined. This will be followed by a consideration of the contribution of various tail-plane arrangements to the characteristics of body-tail combinations.

Wing-body combinations.- The variations with roll angle of the contributions of the wing to the normal force, pitching moment, and rolling moment of two cruciform wing-body configurations having different forebody lengths as obtained both from experiment and from the present theoretical method are presented in figure 10. The corresponding results for the planar wing-body combinations are given in figure 11. Note that these results are referred to the wind-tunnel axis system (see fig. 1(a)) rather than to the body-axis system. It can be observed from figure 10 that the variations in the normal force and pitching moment with roll angle are small even at an angle of pitch of 20° , and the rolling moments are low at all combinations of pitch and roll. It also can be noted that the effect of forebody length is small. A comparison of the theoretical curves with experiment indicates that the present method is adequate for estimating the forces and moments contributed by the wings of a cruciform-wing and body combination. Figure 11 shows that, in contrast to the results for the cruciform wing, the planar wing encounters large changes in the forces and moments with changes in roll angle. Large reductions in the normal force occur, and the rolling moments are high. It is noteworthy that at roll angles between -45° and 45° the rolling moments are of the opposite sign from those for the cruciform combination. This is caused by the fact that at a positive roll angle the positive rolling moment contributed by the vertical wing of the cruciform combination is greater than the negative rolling moment contributed by the horizontal wing. A comparison of the theoretical curves with the experimental results of figure 11 shows that the theoretical method gives an adequate prediction of the normal forces and pitching moments of the planar wing but overestimates the rolling moments. The close agreement for the normal forces and pitching moments stems from the fact that these quantities are proportional to the sum of the normal forces and pitching moments between the left and right wing panels. Thus, the small differences between theory and experiment for the individual panels, as shown in figure 5, are reflected in small differences for the total normal forces and pitching moments in figure 11. The net rolling moments of figure 11, however, represent the differences between the rolling moments on the right panel and those on the left. Therefore, small differences between theory and experiment for the panel rolling moments (fig. 5) lead to large differences for the net rolling moment of a planar-wing configuration. Thus, it appears that the present theoretical method is capable of predicting only the trend but not the magnitude of the rolling moments contributed by a planar wing.

In figure 12 are presented the experimental contributions of the wing panels to the forces and moments on the two planar-wing-body combinations at combined angles of attack and sideslip. The normal-force, pitching-moment, and rolling-moment coefficients are plotted as functions of sideslip angle for several angles of attack for the two panels acting separately

and together. It can be seen that both the normal force and rolling moment of panel 1 increase with angle of sideslip for a given angle of attack. This is caused primarily by the sidewash cross-coupling effect discussed previously, which for this panel increases the panel load (see eq. (A7)). In contrast, the normal force and rolling moment of panel 3 decreases with sideslip angle because of the negative contribution of the cross-coupling effect (see eq. (A8)) and because of the force-reducing effect of the vortex system since panel 3 is close to the left body vortex at large angles of sideslip and small or moderate angles of attack. It is also noted that the pitching moment of panel 1 is relatively independent of sideslip angle and angle of attack whereas the pitching moment of panel 3 becomes more negative with angle of sideslip. This pitching-moment change is also due to the vortex effect as previously discussed. It is seen that the forebody length has little effect on the characteristics of panel 1 but increases the change in the normal force and moments of panel 3 with angle of sideslip. This effect follows from the previously discussed dependence of the strength of the forebody vortices on the forebody length. The total forces contributed by panels 1 and 3, acting together, are indicated by the right-hand curves of figure 12. It can be seen that the normal force decreases with angle of sideslip for a given angle of attack, the pitching moments become more negative, and sizable rolling moments are present. All of these effects are aggravated by an increase in the nose length, as would be expected.

Tail-body combinations.- In order to compare the contribution of various tail-plane arrangements to the stability of tail-body combinations at combined angles of attack and sideslip, the results of figure 4 are presented in figure 13 in terms of the normal-force, side-force, and rolling-moment coefficients contributed by six different panel combinations as indicated by the sketches. The normal-force and side-force results are indicative of the pitching-moment and yawing-moment contributions, respectively, of these tail arrangements.

Consider first the tail-plane arrangements of figures 13(a) to 13(c). It can be seen that for all of these tail combinations the normal-force characteristics are similar. That is, a maximum loss in normal force (or longitudinal stability) due to sideslip occurs at small and moderate angles of attack. It will be recalled from an earlier discussion that this loss is associated primarily with a reduction in the load on the left horizontal panel due to the forebody vortices at large angles of sideslip and small angles of attack.

The side force shows a large loss with angle of attack for the conventional arrangement. In fact, it can be seen that at an angle of attack of about 22° and sideslip of 10° this tail arrangement contributes no side force. Since the side force on a tail surface largely determines the yawing moment contributed by the tail to a complete configuration, it is apparent that the familiar decay in directional stability of current airplanes at high angles of attack is due to this characteristic. In contrast, it can be seen from figure 13(b) that for a configuration having a ventral fin in place of the upper vertical fin, an increase in the side

force, and thus in the yawing moment contributed by the tail plane, occurs as the angle of attack is increased. This difference, of course, arises from the combined effects of differences in the cross-coupling effects due to combined angles of attack and sideslip of these two panels and of the influence of the forebody vortices, as previously discussed. An examination of the side-force characteristics of the cruciform configuration, figure 13(c), shows that the side force is nearly independent of angle of attack, as would be expected from the compensating effects of the upper and lower vertical surfaces.

The rolling-moment results show that the conventional arrangement demonstrates a positive dihedral effect (negative C_{lp}) and that the rolling moment increases with angle of attack at 20° angle of sideslip. The configuration with the ventral fin, on the other hand, shows a negative dihedral effect which decreases with angle of attack. It is noted that the rolling moments for the + configuration are small throughout the angle-of-attack and -sideslip ranges. However, a sign reversal in the rolling moment occurs at a sideslip angle of 10° .

Now consider the configurations shown in figures 13(d) to 13(f). It can be noted that both the V tail and the inverted V tail exhibit a shift in the normal-force curves with angle of sideslip but in opposite directions. This effect would lead to undesirable longitudinal-trim changes due to sideslip. In addition, the V tail exhibits a serious loss in effectiveness at angles of attack above about 12° , as indicated by the reduction in the normal-force-curve slope. It is seen that the X arrangement, however, exhibits reasonably good longitudinal-stability characteristics; that is, the change in normal force with angle of sideslip is relatively small and regular. The side-force, or directional stability, characteristics of all three configurations are seen to be desirable; that is, the side force is essentially independent of angle of attack. The rolling-moment results show that the rolling moment at zero angle of attack for both the V and inverted V tails is considerably larger than for their counterparts of figures 13(a) and 13(b), but that in both cases, these rolling moments diminish with angle of attack. The rolling-moment curves of the X configuration of figure 13(f) are similar to but of opposite sign from those of the cruciform tail of figure 13(c).

From a comparison of the curves shown in figure 13, it is clear that only three of these tail-plane arrangements can be expected to contribute desirable stability characteristics: a horizontal tail in combination with a ventral fin, a + tail, or an X tail. This follows from the fact that the longitudinal stability contributed by each of these tails would be nearly independent of sideslip angle and the directional stability would remain nearly constant or increase with angle of attack. It should be noted that each of these tail-plane arrangements derives its favorable stability characteristics from one or two panels extending below the body. In a practical design, however, the size of such panels might be restricted by ground-clearance considerations, and the adverse dihedral effect of these configurations must be considered.

CONCLUSIONS

Wind-tunnel tests were conducted at a Mach number of 1.96 over a wide range of combined angles of pitch and roll to investigate the normal forces, pitching moments, and rolling moments acting on each wing panel of a wing-body combination having an aspect-ratio-2 triangular cruciform wing. On the basis of the results of these tests and of a concurrent theoretical study, the following conclusions have been drawn:

1. Large changes in the panel forces and moments can occur as the result of combined angles. These changes are caused primarily by a cross coupling between the sidewash velocities due to angle of attack and sideslip and by the presence of crossflow separation vortices from the forebody. An increase in the forebody length increases the effect of the body vortices on the panel forces and moments. The forces and moments on each wing panel of a cruciform-wing and body combination are influenced to an appreciable degree by only one of the other panels, namely, the adjacent surface on the windward side of the body. A satisfactory prediction of the wing-panel characteristics at combined angles can be achieved through the use of a calculative method based on slender-body and strip theories. This method requires only a knowledge of the wing-alone characteristics and the initial positions of the forebody vortices.

2. The normal force and pitching moment contributed by the wing of a cruciform-wing and body combination at any angle of pitch are essentially independent of roll angle, and the rolling moments are small. The normal force and pitching moment contributed by the wing of a planar-wing and body combination at an angle of attack diminish with sideslip angle, and large rolling moments occur.

3. The directional stability contributed by a conventional arrangement of tail surfaces on a body decreases seriously with angle of attack, especially at small sideslip angles. However, the opposite trend occurs when the vertical fin is replaced by a ventral (lower vertical) fin. A V and an inverted V tail arrangement give a directional-stability contribution which is nearly independent of angle of attack, but these tails may produce undesirable longitudinal trim changes and large rolling moments due to sideslip. A + and an X tail exhibit longitudinal- and directional-stability characteristics which are desirably independent of angle of sideslip and angle of attack; however, the rolling moments, although relatively small in magnitude, show a reversal with increasing angles of attack.

Ames Aeronautical Laboratory
National Advisory Committee for Aeronautics
Moffett Field, Calif., Sept. 12, 1957

APPENDIX A

FORCES AND MOMENTS ON WING PANELS OF WING-
BODY COMBINATIONS IN POTENTIAL FLOW

Expressions have been derived by means of slender-body theory in Appendix A of reference 3 for the differential pressures acting on wing-body combinations at combined angles of attack α and sideslip β . The pressure difference across the horizontal and vertical wing panels of a cruciform combination having four identical wing panels in combination with a circular cylinder is given by

$$\left(\frac{\Delta p}{q}\right)_1 = \frac{4\alpha\left(1 - \frac{a^4}{s^4}\right) \frac{ds}{dx}}{\left[\left(1 + \frac{a^4}{s^4}\right) - \frac{y^2}{s^2} \left(1 + \frac{a^4}{y^4}\right)\right]^{1/2}} + \frac{4\alpha\beta\left(\frac{y}{s}\right)^2 \left(1 - \frac{a^4}{y^4}\right)^2}{\left[\left(1 + \frac{a^4}{s^4}\right)^2 - \frac{y^4}{s^4} \left(1 + \frac{a^4}{y^4}\right)^2\right]^{1/2}} \quad (A1)$$

$$\left(\frac{\Delta p}{q}\right)_3 = \frac{4\alpha\left(1 - \frac{a^4}{s^4}\right) \frac{ds}{dx}}{\left[\left(1 + \frac{a^4}{s^4}\right) - \frac{y^2}{s^2} \left(1 + \frac{a^4}{y^4}\right)\right]^{1/2}} - \frac{4\alpha\beta\left(\frac{y}{s}\right)^2 \left(1 - \frac{a^4}{y^4}\right)^2}{\left[\left(1 + \frac{a^4}{s^4}\right)^2 - \frac{y^4}{s^4} \left(1 + \frac{a^4}{y^4}\right)^2\right]^{1/2}} \quad (A2)$$

$$\left(\frac{\Delta p}{q}\right)_4 = \frac{-4\beta\left(1 - \frac{a^4}{s^4}\right) \frac{ds}{dx}}{\left[\left(1 + \frac{a^4}{s^4}\right) - \frac{z^2}{s^2} \left(1 + \frac{a^4}{z^4}\right)\right]^{1/2}} + \frac{4\alpha\beta\left(\frac{z}{s}\right)^2 \left(1 - \frac{a^4}{z^4}\right)^2}{\left[\left(1 + \frac{a^4}{s^4}\right)^2 - \frac{z^4}{s^4} \left(1 + \frac{a^4}{z^4}\right)^2\right]^{1/2}} \quad (A3)$$

$$\left(\frac{\Delta p}{q}\right)_2 = \frac{-4\beta\left(1 - \frac{a^4}{s^4}\right) \frac{ds}{dx}}{\left[\left(1 + \frac{a^4}{s^4}\right) - \frac{z^2}{s^2} \left(1 + \frac{a^4}{z^4}\right)\right]^{1/2}} - \frac{4\alpha\beta\left(\frac{z}{s}\right)^2 \left(1 - \frac{a^4}{z^4}\right)^2}{\left[\left(1 + \frac{a^4}{s^4}\right)^2 - \frac{z^4}{s^4} \left(1 + \frac{a^4}{z^4}\right)^2\right]^{1/2}} \quad (A4)$$

and the pressure difference across the horizontal panels of a planar combination is given by

$$\left(\frac{\Delta p}{q}\right)_1 = \frac{4\alpha \left(1 - \frac{a^4}{s^4}\right) \frac{ds}{dx}}{\left[\left(1 + \frac{a^4}{s^4}\right) - \frac{y^2}{s^2} \left(1 + \frac{a^4}{y^4}\right)\right]^{1/2}} + \frac{4\alpha\beta \frac{y}{a} \left(1 - \frac{a^2}{y^2}\right) \left(1 - \frac{a^4}{y^4}\right) \frac{s}{a}}{\left[\left(\frac{s^2}{a^2} - \frac{y^2}{a^2}\right) \left(\frac{s^2}{a^2} - \frac{a^2}{y^2}\right)\right]^{1/2}} \quad (A5)$$

$$\left(\frac{\Delta p}{q}\right)_3 = \frac{4\alpha \left(1 - \frac{a^4}{s^4}\right) \frac{ds}{dx}}{\left[\left(1 + \frac{a^4}{s^4}\right) - \frac{y^2}{s^2} \left(1 + \frac{a^4}{y^4}\right)\right]^{1/2}} - \frac{4\alpha\beta \frac{y}{a} \left(1 - \frac{a^2}{y^2}\right) \left(1 - \frac{a^4}{y^4}\right) \frac{s}{a}}{\left[\left(\frac{s^2}{a^2} - \frac{y^2}{a^2}\right) \left(\frac{s^2}{a^2} - \frac{a^2}{y^2}\right)\right]^{1/2}} \quad (A6)$$

The normal force and moments acting on each wing panel are determined from integrations involving these equations over the panel plan-form area. The resulting normal force, pitching moment, and rolling moment on the horizontal panels of either a cruciform or a planar wing-body combination may be expressed by

$$C_{N_1} = C_{N_{\alpha, w(\beta=0)}} \left(K_w \alpha + \frac{K_\phi}{\tan \epsilon} \alpha \beta \right) \quad (A7)$$

$$C_{N_3} = C_{N_{\alpha, w(\beta=0)}} \left(K_w \alpha - \frac{K_\phi}{\tan \epsilon} \alpha \beta \right) \quad (A8)$$

$$C_{m_1} = -C_{N_{\alpha, w(\beta=0)}} \left[K_w \left(\frac{x_{cp}}{\bar{c}} \right)_\alpha + \frac{K_\phi}{\tan \epsilon} \left(\frac{x_{cp}}{\bar{c}} \right)_\phi \alpha \beta \right] \quad (A9)$$

$$C_{m_3} = -C_{N_{\alpha, w(\beta=0)}} \left[K_w \left(\frac{x_{cp}}{\bar{c}} \right)_\alpha - \frac{K_\phi}{\tan \epsilon} \left(\frac{x_{cp}}{\bar{c}} \right)_\phi \alpha \beta \right] \quad (A10)$$

$$C_{l_1} = -C_{N_{\alpha, w(\beta=0)}} \left[K_w \left(\frac{y_{cp}}{s_m} \right)_\alpha + \frac{K_\phi}{\tan \epsilon} \left(\frac{y_{cp}}{s_m} \right)_\phi \alpha \beta \right] \quad (A11)$$

$$C_{l_3} = C_{N_{\alpha, w(\beta=0)}} \left[K_w \left(\frac{y_{cp}}{s_m} \right)_{\alpha} - \frac{K_{\phi}}{\tan \epsilon} \left(\frac{y_{cp}}{s_m} \right)_{\phi} \alpha \beta \right] \quad (A12)$$

and for the vertical panels, the expressions for the side force, yawing moments, and rolling moment by

$$C_{Y_4} = C_{Y_{\beta, w(\alpha=0)}} \left(K_w \beta - \frac{K_{\phi}}{\tan \epsilon} \alpha \beta \right) \quad (A13)$$

$$C_{Y_2} = C_{Y_{\beta, w(\alpha=0)}} \left(K_w \beta + \frac{K_{\phi}}{\tan \epsilon} \alpha \beta \right) \quad (A14)$$

$$C_{n_4} = -C_{Y_{\beta, w(\alpha=0)}} \left[K_w \left(\frac{x_{cp}}{\bar{c}} \right)_{\alpha} \beta - \frac{K_{\phi}}{\tan \epsilon} \left(\frac{x_{cp}}{\bar{c}} \right)_{\phi} \alpha \beta \right] \quad (A15)$$

$$C_{n_2} = -C_{Y_{\beta, w(\alpha=0)}} \left[K_w \left(\frac{x_{cp}}{\bar{c}} \right)_{\alpha} \beta + \frac{K_{\phi}}{\tan \epsilon} \left(\frac{x_{cp}}{\bar{c}} \right)_{\phi} \alpha \beta \right] \quad (A16)$$

$$C_{l_4} = C_{Y_{\beta, w(\alpha=0)}} \left[K_w \left(\frac{y_{cp}}{s_m} \right)_{\alpha} \beta - \frac{K_{\phi}}{\tan \epsilon} \left(\frac{y_{cp}}{s_m} \right)_{\phi} \alpha \beta \right] \quad (A17)$$

$$C_{l_2} = -C_{Y_{\beta, w(\alpha=0)}} \left[K_w \left(\frac{y_{cp}}{s_m} \right)_{\alpha} \beta + \frac{K_{\phi}}{\tan \epsilon} \left(\frac{y_{cp}}{s_m} \right)_{\phi} \alpha \beta \right] \quad (A18)$$

The factors K_w , K_{ϕ} , $(y_{cp}/s_m)_{\alpha}$, and $(y_{cp}/s_m)_{\phi}$ depend only on the quantity a/s_m and are independent of the plan-form shape but $(x_{cp}/\bar{c})_{\alpha}$ and $(x_{cp}/\bar{c})_{\phi}$ depend on both a/s_m and the plan-form shape. The factor K_w is given by the ratio of the normal force on the panel in the presence of the body at zero sideslip to the corresponding force on the panel alone. The normal force in the presence of the body at zero sideslip is obtained from an integration of the first term of the loading equations (A1) to (A6) over the panel, and the force on the panel alone is obtained from an integration of this term with the body radius a set equal to zero. The longitudinal

and lateral center-of-pressure factors $(x_{cp}/c_r)_\alpha$ and $(y_{cp}/s_m)_\alpha$ are given by the ratio of the pitching and rolling moments, respectively, of the panel in the presence of the body at zero sideslip to the corresponding normal force. These moments are obtained from an integration of the product of the loading (given by the first term of eqs. (A1) to (A6)) and the appropriate moment arm. The results may be expressed by

$$K_W = \frac{1}{\pi \left(\frac{s_m}{a} - 1 \right)^2} \left[\frac{\pi}{2} \left(\frac{s_m}{a} - \frac{a}{s_m} \right)^2 - 2 \left(\frac{s_m}{a} - \frac{a}{s_m} \right) + \left(\frac{s_m}{a} + \frac{a}{s_m} \right)^2 \sin^{-1} \frac{s_m^2 - a^2}{s_m^2 + a^2} \right] \quad (A19)$$

$$\left(\frac{x_{cp}}{c_r} \right)_\alpha = \frac{2 \left(\frac{1}{3} + \frac{a^4}{s_m^4} \right) \tan^{-1} \frac{a}{s_m} + \frac{2}{3} \frac{a^3}{s_m^3} \ln \left[\left(\frac{s_m^2 + a^2}{2s_m^2} \right)^2 \frac{s_m}{a} \right] - \frac{1}{3} \frac{a^3}{s_m^3} \left(2\pi - 1 + \frac{s_m^2}{a^2} \right)}{\left(1 - \frac{a}{s_m} \right) \left\{ \left(1 + \frac{a^2}{s_m^2} \right)^2 \tan^{-1} \frac{s_m}{a} - \frac{a^2}{s_m^2} \left[\pi + \left(\frac{s_m}{a} - \frac{a}{s_m} \right) \right] \right\}} - \frac{\frac{a}{s_m}}{1 - \frac{a}{s_m}} \quad (A20)$$

$$\left(\frac{y_{cp}}{s_m} \right)_\alpha = \frac{2}{3\pi K_W \frac{s_m^4}{a^4} \left(\frac{s_m}{a} - 1 \right)^2} \left\{ \frac{s_m}{a} \left(\frac{s_m^2}{a^2} + 1 \right) \left(\frac{s_m}{a} - \frac{s_m^2}{a^2} + 1 \right) K \left[\left(\frac{s_m - a}{s_m + a} \right)^2 \right] + \right. \\ \left. \left(\frac{s_m}{a} + 1 \right)^2 \left(\frac{s_m^4}{a^4} + 1 \right) E \left[\left(\frac{s_m - a}{s_m + a} \right)^2 \right] + \left(\frac{s_m^2}{a^2} + 1 \right)^3 \right\} \quad (A21)$$

Although equations (A19) and (A20) have been derived previously in references 5 and 1, respectively, these equations are presented here for completeness. Equations (A19) to (A21) are applicable to either cruciform or planar configurations having wing panels with the same span. Equations (A19) and (A21) are applicable to any slender plan form having an

unswept trailing edge, but equation (A20) is restricted to a triangular plan form. Figure 3(a) shows the variation of these quantities with a/s_m . The factor K_ϕ is proportional to the ratio of the normal force on the panel in the presence of the body due to combined angles of attack and sideslip to the normal force on the panel alone at zero sideslip and at the same angle of attack. The first quantity is obtained from an integration of the second term of equations (A1) to (A6) over the panel, and the latter quantity from an integration of the first term with the body radius a set equal to zero. The center-of-pressure factors $(x_{cp}/c_r)_\phi$ and $(y_{cp}/s_m)_\phi$ are obtained in exactly the same manner as the factors $(x_{cp}/c_r)_\alpha$ and $(y_{cp}/s_m)_\alpha$ previously described, with the exception that the second term in equations (A1) to (A6) is used in place of the first term.

Because of the effects of panel-panel interference at combined angles, it is necessary to distinguish between cruciform and planar configurations since the loading expressions are different. Thus, for a cruciform configuration

$$K_\phi = \frac{1}{\pi \left(\frac{s_m}{a} - 1 \right)^2} \int_1^{\frac{s_m^2}{a^2}} \frac{1}{\delta^3} \left[\frac{(\delta^2 - 1)^3}{2} \right]^{1/2} [F(\psi_1, k_1) + F(\psi_2, k_2)] d\delta \quad (A22)$$

$$\left(\frac{x_{cp}}{c_r} \right)_\phi = \frac{1}{2\pi \left(\frac{s_m}{a} - 1 \right)^3 K_\phi} \int_1^{\frac{s_m^2}{a^2}} \frac{(\delta^2 - 1)^2}{\delta^{7/2}} \ln \frac{2\delta \sqrt{\left(1 - \delta^2 \frac{s_m^4}{a^4} \right) \left(\delta^2 - \frac{s_m^4}{a^4} \right)} - \left(\delta^4 - 2 \frac{s_m^4}{a^4} \delta^2 + 1 \right)}{\delta^4 - 1} d\delta - \frac{\frac{a}{s_m}}{1 - \frac{a}{s_m}} \quad (A23)$$

$$\left(\frac{y_{cp}}{s_m} \right)_\phi = \frac{1}{\pi \frac{s_m}{a} \left(\frac{s_m}{a} - 1 \right)^2 K_\phi} \int_1^{\frac{s_m^2}{a^2}} \left[\frac{(\delta^2 - 1)^3}{2\delta^5} \right]^{1/2} [F(\psi_1, k_1) + F(\psi_2, k_2)] d\delta \quad (A24)$$

and for a planar configuration

$$K_\phi = \frac{2}{\pi \left(\frac{s_m}{a} - 1 \right)^2} \int_1^{\frac{s_m^2}{a^2}} \frac{(\delta - 1)(\delta^2 - 1)}{\delta^3} \tanh^{-1} \left(\frac{\frac{s_m^2}{a^2} - \delta}{\frac{s_m^2}{a^2} - \frac{1}{\delta}} \right)^{1/2} d\delta \quad (A25)$$

$$\left(\frac{x_{cp}}{c_r}\right)_\varphi = \frac{2}{\pi \left(\frac{s_m}{a} - 1\right)^3 K_\varphi} \int_1^{\frac{s_m^2}{a^2}} \frac{(\delta - 1)(\delta^2 - 1)}{\delta^{5/2}} \left[F(\psi_3, k_3) - E(\psi_3, k_3) + \frac{s_m}{a} \left(\frac{\frac{s_m^2}{a^2} - \delta}{\frac{s_m^2}{a^2} \delta - 1} \right)^{1/2} \right] d\delta - \frac{\frac{a}{s_m}}{1 - \frac{a}{s_m}} \quad (A26)$$

$$\left(\frac{y_{cp}}{s_m}\right)_\varphi = \frac{1}{\pi \frac{s_m}{a} \left(\frac{s_m}{a} - 1\right)^2 K_\varphi} \int_1^{\frac{s_m^2}{a^2}} \frac{(\delta - 1)(\delta^2 - 1)}{\delta^{5/2}} \tanh^{-1} \left(\frac{\frac{s_m^2}{a^2} - \delta}{\frac{s_m^2}{a^2} - \frac{1}{\delta}} \right)^{1/2} d\delta \quad (A27)$$

where

$$\delta = \frac{y^2}{a^2}$$

$$\psi_1 = \cos^{-1} \frac{\delta + 1}{\left(\frac{s_m}{a} + \frac{a}{s_m}\right) \sqrt{\delta}}$$

$$k_1 = \frac{\delta - 1}{[2(\delta^2 + 1)]^{1/2}}$$

$$\psi_2 = \cos^{-1} \frac{\delta - 1}{\left(\frac{s_m}{a} - \frac{a}{s_m}\right) \sqrt{\delta}}$$

$$k_2 = \frac{\delta + 1}{[2(\delta^2 + 1)]^{1/2}}$$

$$\psi_3 = \sin^{-1} \left(\frac{\frac{s_m^2}{a^2} - \delta}{\frac{s_m^2}{a^2} - \frac{1}{\delta}} \right)^{1/2}$$

$$k_3 = \frac{1}{\delta}$$

The integrations indicated in equations (A22) to (A27) have been performed numerically, and the resulting variations in K_ϕ , $(x_{cp}/c_r)_\phi$, and $[(y_{cp}-a)/(s_m-a)]_\phi$ with a/s_m are presented in figure 3(b) for both cruciform and planar configurations. The same plan-form restrictions apply to these quantities as for K_W , $(x_{cp}/c_r)_\alpha$, and $(y_{cp}/s_m)_\alpha$ discussed previously.

APPENDIX B

EFFECT OF BODY VORTICES ON WING-PANEL

FORCES AND MOMENTS

The normal force, pitching moment, and rolling moment on the right wing panel due to a vortex of known strength and position can be computed from strip theory by

$$C_N = C_{N_{\alpha_w}} \frac{a^2}{S} \int_1^{\frac{s_m}{a}} \frac{w}{V} \left(\frac{c}{a} \right) d \left(\frac{y}{a} \right) \quad (B1)$$

$$C_m = -C_{N_{\alpha_w}} \frac{a^3}{S \bar{c}} \int_1^{\frac{s_m}{a}} \frac{w}{V} \left(\frac{c}{a} \right) \frac{x_{cp}}{a} d \left(\frac{y}{a} \right) \quad (B2)$$

$$C_l = -C_{N_{\alpha_w}} \frac{a^3}{S s_m} \int_1^{\frac{s_m}{a}} \frac{w}{V} \left(\frac{c}{a} \right) \frac{y}{a} d \left(\frac{y}{a} \right) \quad (B3)$$

The factor $C_{N_{\alpha_w}}$ represents the normal-force-curve slope of a two-dimensional wing having a sweepback of $\Lambda - \beta$. The spanwise distribution of upwash induced by an incompressible inviscid two-dimensional vortex is given by

$$\frac{w}{V} = \frac{\Gamma}{2\pi V} \frac{y - y_v}{z_v^2 + (y - y_v)^2} \quad (B4)$$

The spanwise variation of the chord of a general plan form having straight edges can be expressed by

$$\frac{c}{a} = A - B \frac{y}{a} \quad (B5)$$

where

$$A = \frac{c_o}{a}$$

$$B = \frac{c_o}{s_m} (1-\lambda)$$

and the longitudinal center-of-pressure location of each strip of constant loading by

$$\frac{x_{cp}}{a} = C + D \frac{y}{a} \quad (B6)$$

where

$$C = \frac{c_o}{2a} - \tan \Lambda$$

$$D = \tan \Lambda - \frac{c_o}{2s} (1-\lambda)$$

If equations (B4), (B5), and (B6) are substituted into (B1), (B2), and (B3), and the integrations are performed,

$$C_N = C_{N_{\alpha_w}} \frac{a^2}{S} \frac{\Gamma}{2\pi Va} \left[B \left(\frac{s_m}{a} - 1 \right) + \frac{1}{2} \left(A - B \frac{y_v}{a} \right) f_1 - B \frac{z_v}{a} f_2 \right] \quad (B7)$$

$$C_m = -C_{N_{\alpha_w}} \frac{a^3}{S \bar{c}} \frac{\Gamma}{2\pi Va} \left\{ \frac{1}{2} BD \left(\frac{s_m^2}{a^2} - 1 \right) + \left(AD + BC + BD \frac{y_v}{a} \right) \left(\frac{s_m}{a} - 1 \right) - \right.$$

$$\left. \frac{1}{2} \left[BD \left(\frac{z_v^2}{a^2} - \frac{y_v^2}{a^2} \right) - (AD + BC) \frac{y_v}{a} - AC \right] f_1 - \left(AD + BC + 2BD \frac{y_v}{a} \right) \frac{z_v}{a} f_2 \right\} \quad (B8)$$

$$C_l = -C_{N\alpha_w} \frac{a^3}{s s_m} \frac{\Gamma}{2\pi V a} \left[\frac{1}{2} B \left(\frac{s_m^2}{a^2} - 1 \right) + \left(A + B \frac{y_v}{a} \right) \left(\frac{s_m}{a} - 1 \right) + \right. \\ \left. \frac{1}{2} \left(A \frac{y_v}{a} + B \frac{y_v^2}{a^2} - B \frac{z_v^2}{a^2} \right) f_1 - \left(A + 2B \frac{y_v}{a} \right) \frac{z_v}{a} f_2 \right] \quad (B9)$$

where

$$f_1 = \ln \frac{z_v^2 + (s_m - y_v)^2}{z_v^2 + (a - y_v)^2}$$

$$f_2 = \tan^{-1} \frac{s_m - y_v}{z_v} - \tan^{-1} \frac{a - y_v}{z_v}$$

REFERENCES

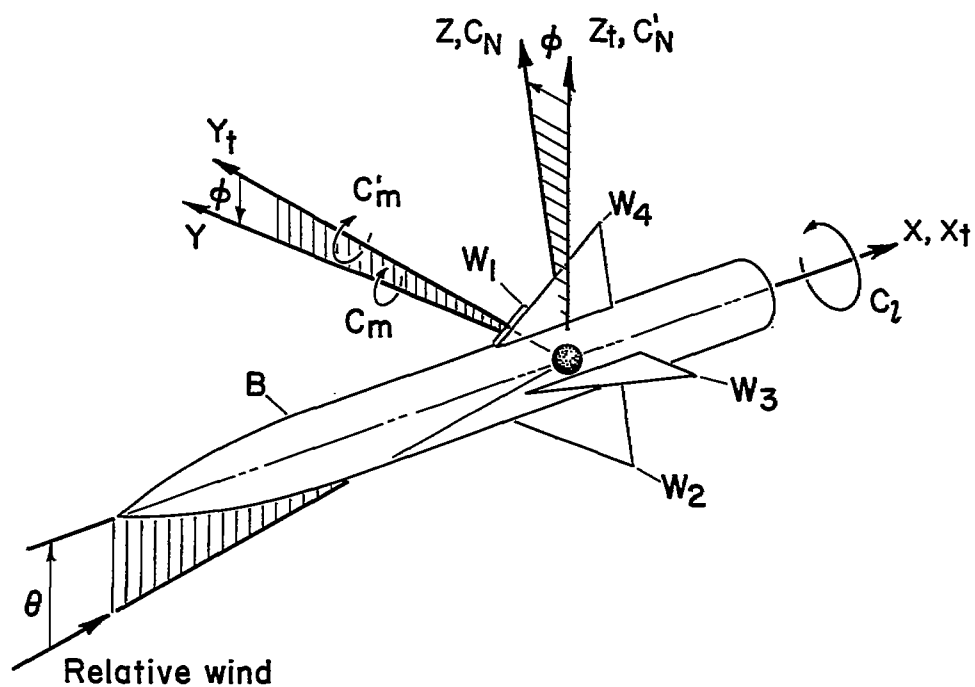
1. Pitts, William C., Nielsen, Jack N., and Kaattari, George E.: Lift and Center of Pressure of Wing-Body-Tail Combinations at Subsonic, Transonic, and Supersonic Speeds. NACA Rep. 1307, 1957.
2. Spreiter, John R.: The Aerodynamic Forces on Slender Plane- and Cruciform-Wing and Body Combinations. NACA Rep. 962, 1950.
3. Spreiter, John R., and Sacks, Alvin H.: A Theoretical Study of the Aerodynamics of Slender Cruciform-Wing Arrangements and Their Wakes. NACA Rep. 1296, 1957. (Supersedes NACA TN 3528)
4. Jorgensen, Leland H., and Perkins, Edward W.: Investigation of Some Wake Vortex Characteristics of an Inclined Ogive-Cylinder Body at Mach Number 1.98. NACA RM A55E31, 1955.
5. Morikawa, George: Supersonic Wing-Body Lift. Jour. Aero. Sci., vol. 18, no. 4, Apr. 1951, pp. 217-228.

TABLE I.- GEOMETRIC CHARACTERISTICS OF MODEL

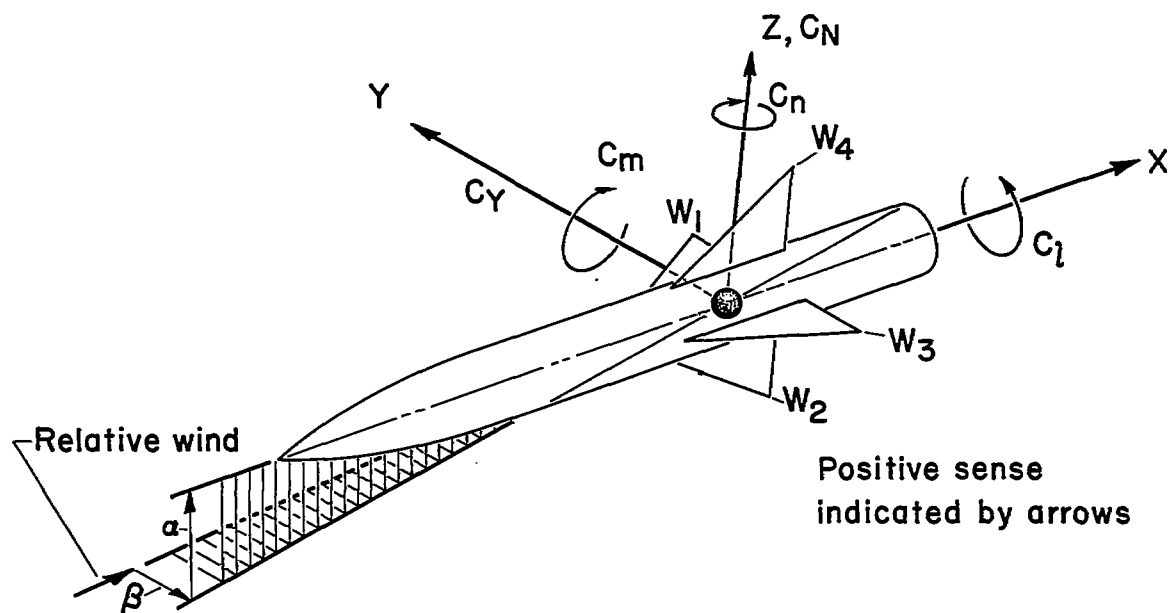
Body	
Maximum diameter, in.	1.50
Length, in.	
With long forebody	15.56
With short forebody	11.06
Fineness ratio	
With long forebody	10.4
With short forebody	7.4
Exposed wing panels	
Plan-form area (per pair), sq in.	8.00
Chord at body juncture	4.00
Mean aerodynamic chord, in.	2.67
Span, in.	2.00
Aspect ratio (per pair)	2
Maximum thickness	0.05c
Position of maximum thickness	0.50c
Trailing-edge thickness	0.025c

TABLE II.- EXPERIMENTAL NORMAL-FORCE CHARACTERISTICS OF WING ALONE; $\beta=0$,
 $R = 1.03 \times 10^6$, $M = 1.97$

α , deg	C_{Nw}
0	0
3	.086
6	.192
10	.333
15	.492
20	.644
25	.808
30	.982

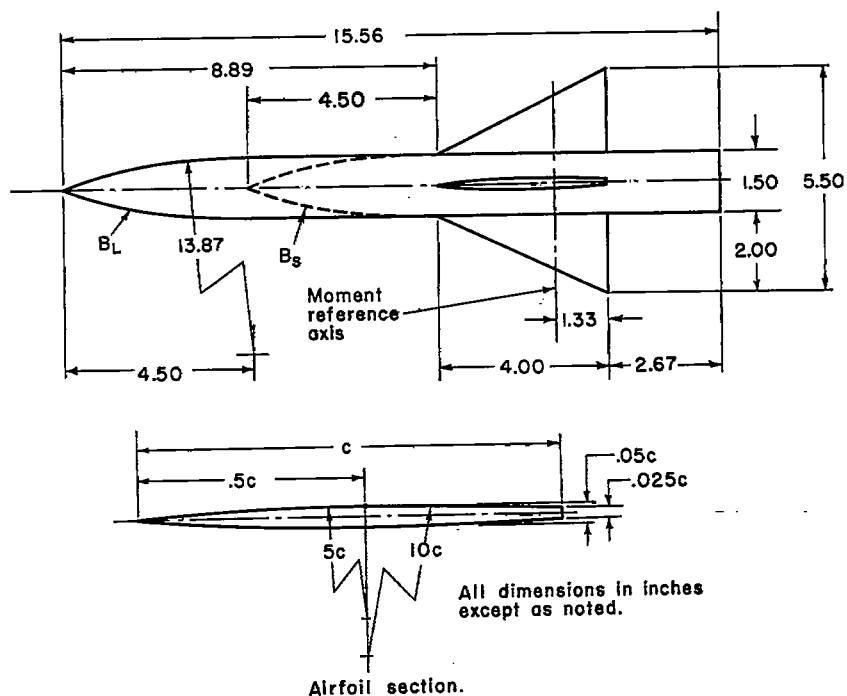


(a) Wind-tunnel axis system.

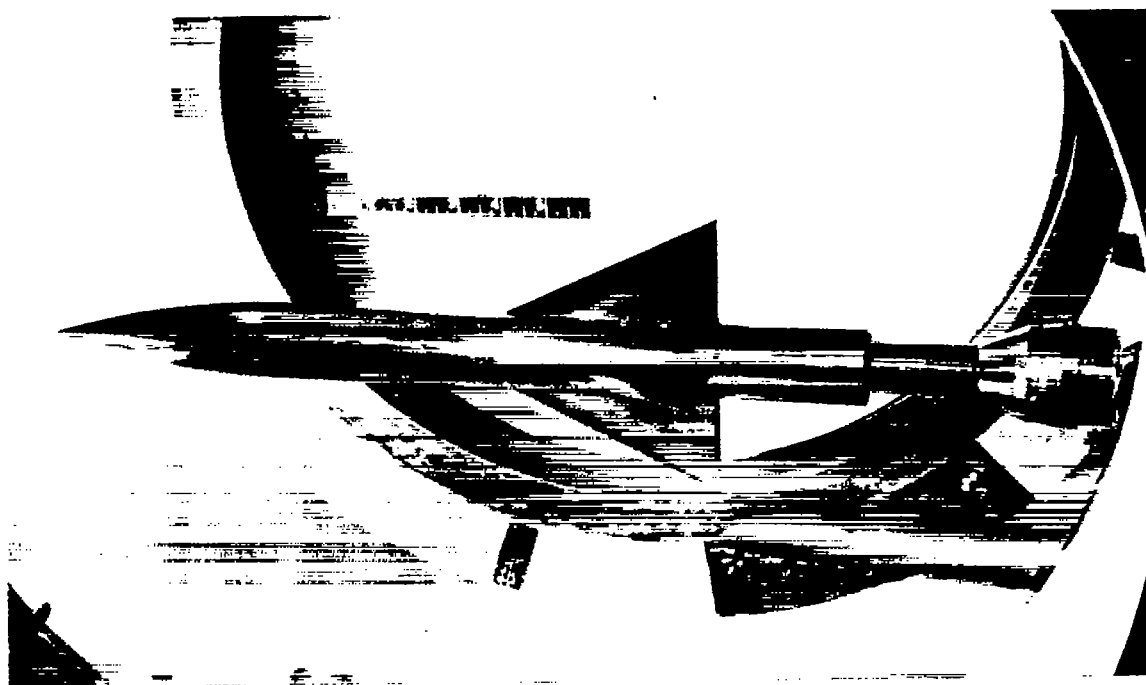


(b) Body axis system.

Figure 1.- Coordinate axis systems.



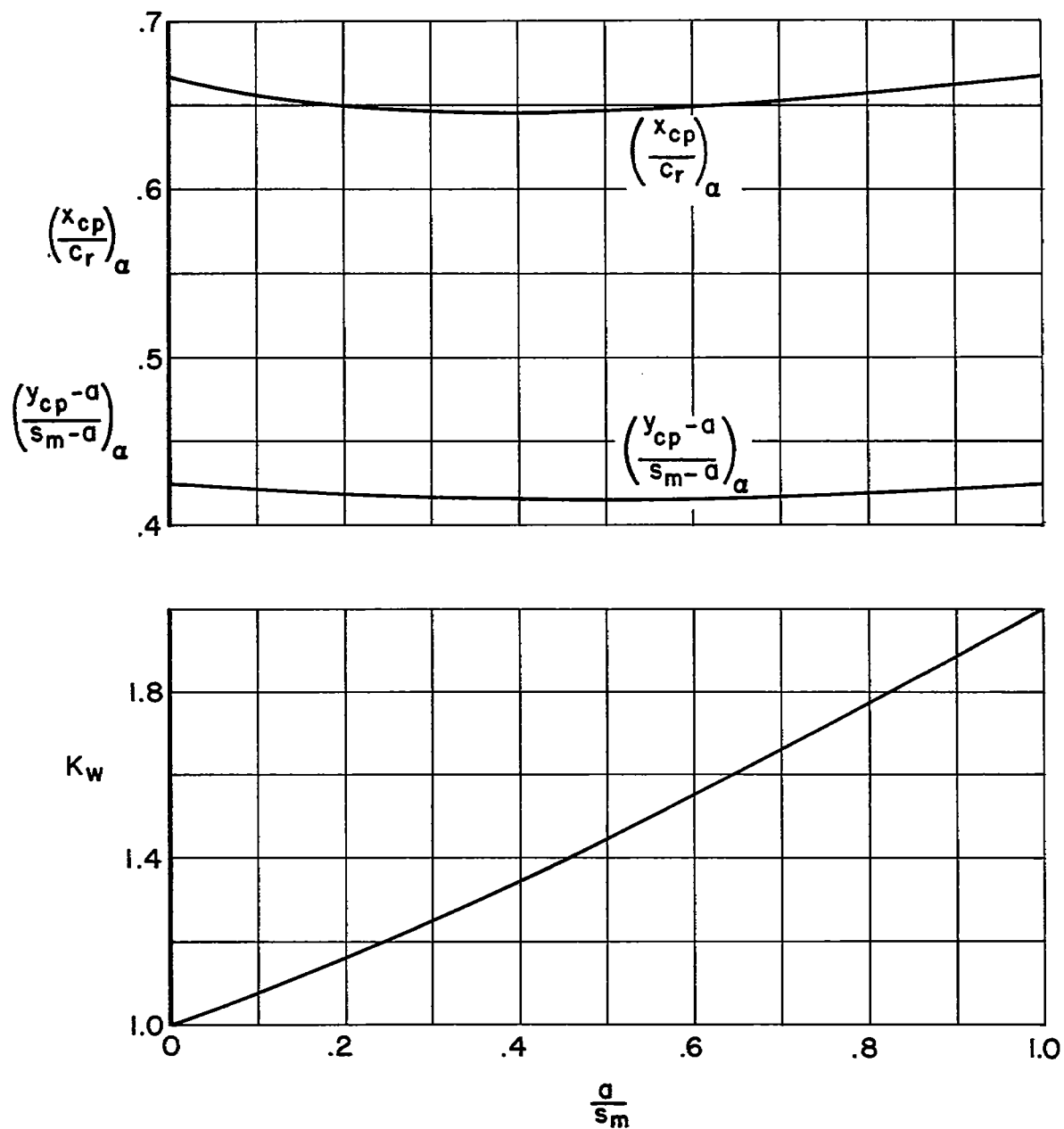
(a) Model geometry.



(b) View of model in wind tunnel.

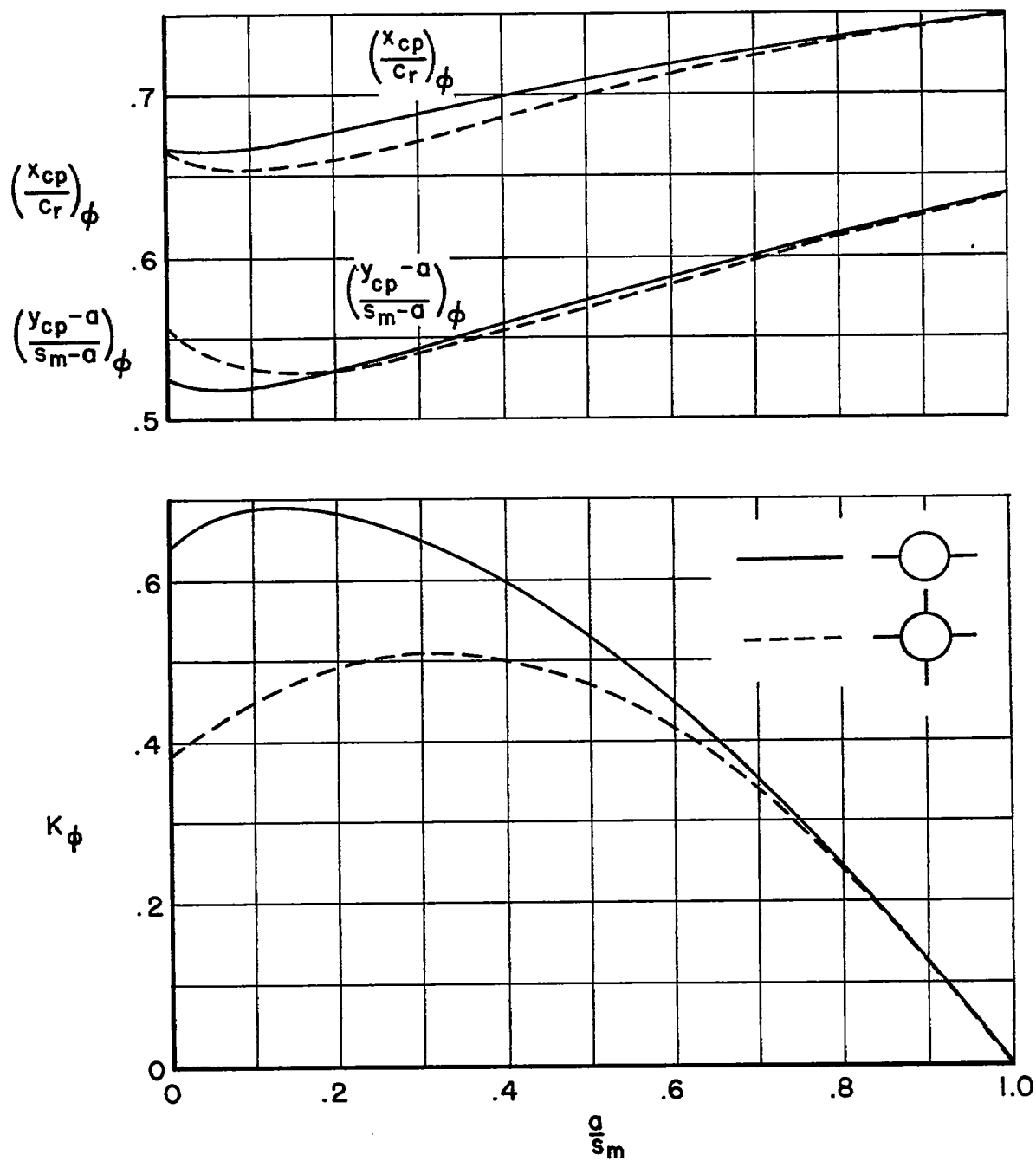
A-18907

Figure 2.- Model.



(a) Effects of angle of attack or sideslip.

Figure 3.- Theoretical center-of-pressure and normal-force parameters for wing panels of wing-body combinations.



(b) Effects of combined angles of attack and sideslip.

Figure 3.- Concluded.

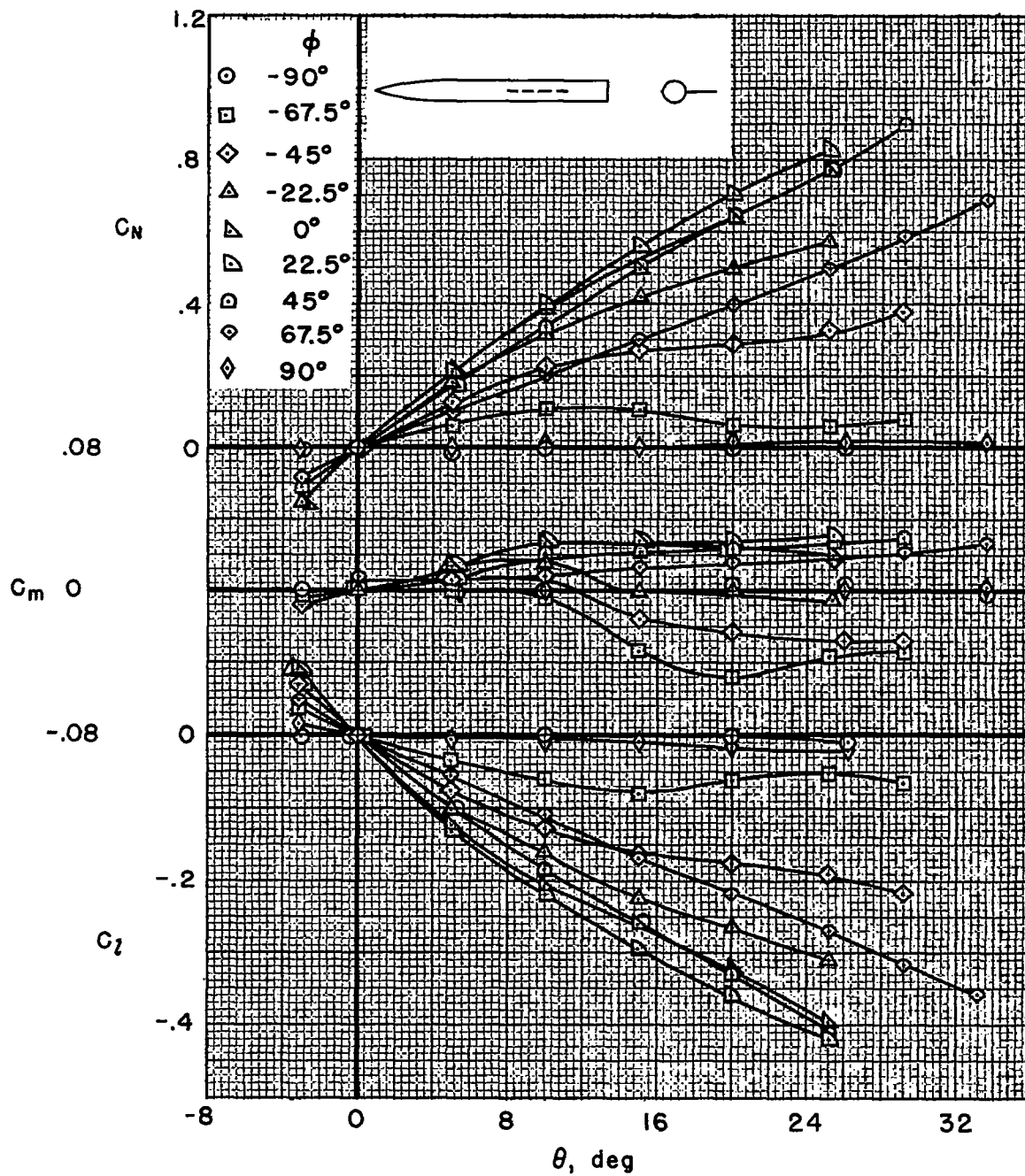
(a) $W_1(B_L)$ configuration.

Figure 4.- Aerodynamic characteristics of wing panel W_1 ; $R = 1.03 \times 10^6$.

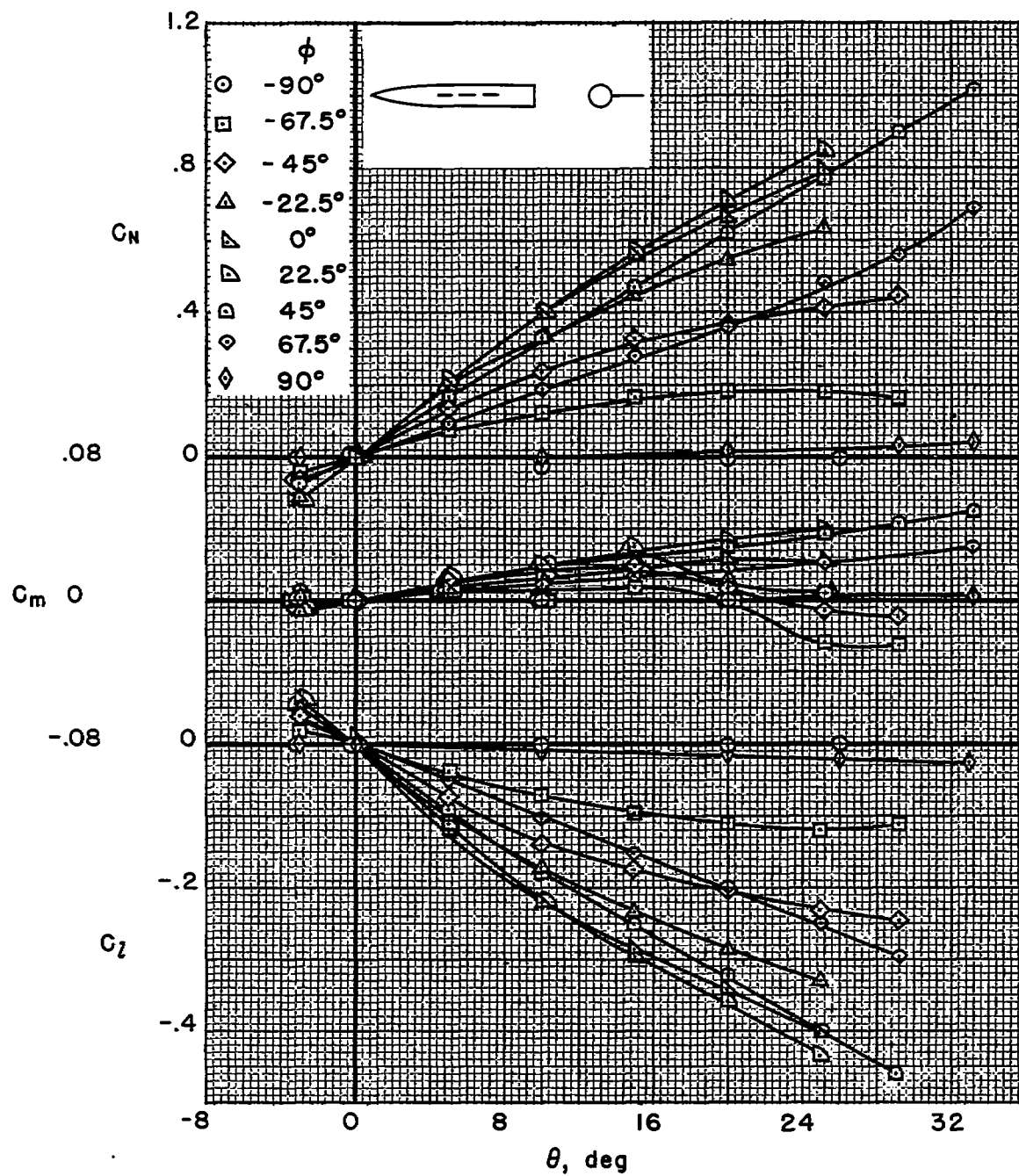
(b) $W_1(B_S)$ configuration.

Figure 4.- Continued.

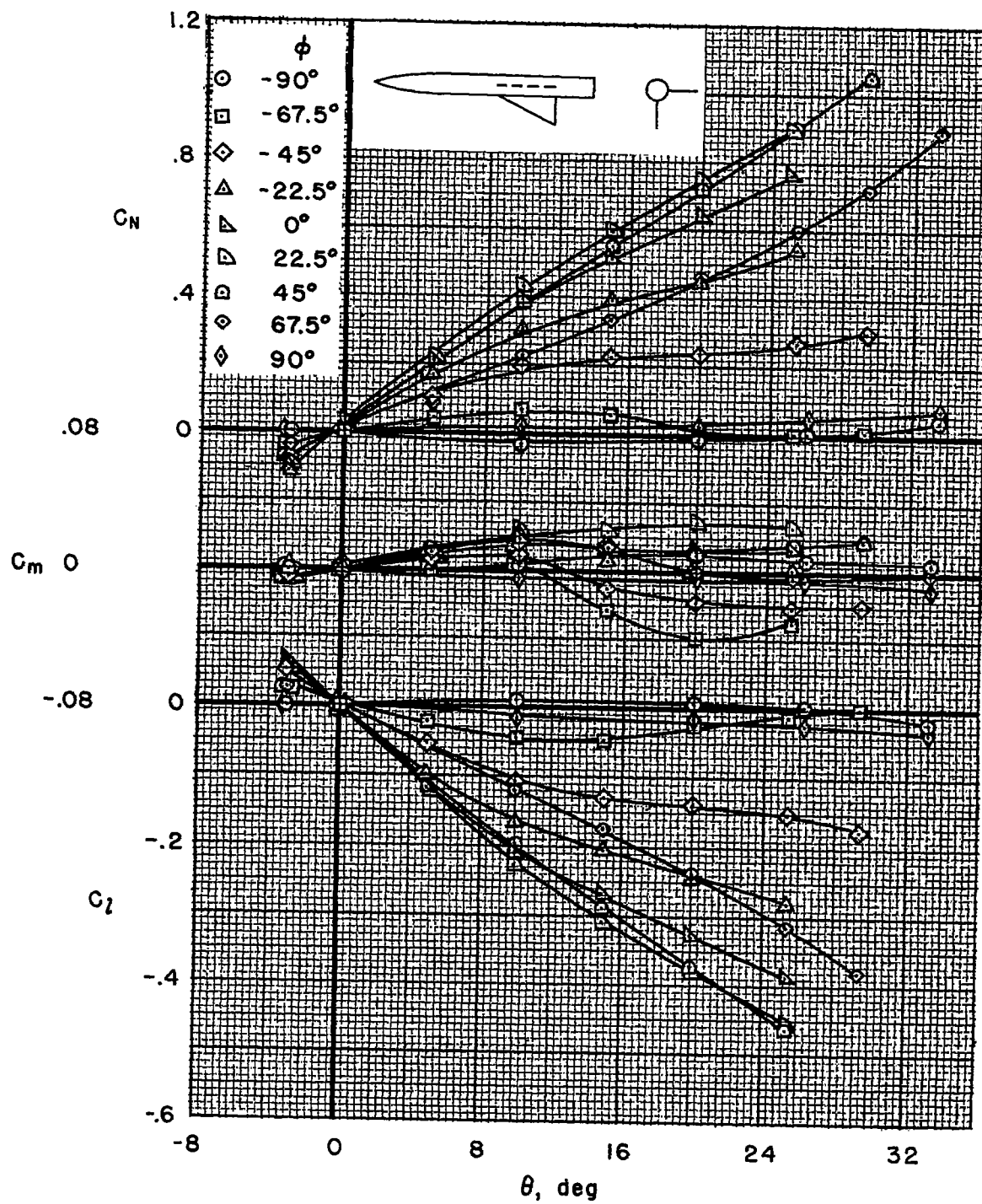
(c) $W_1(B_LW_2)$ configuration.

Figure 4.- Continued.

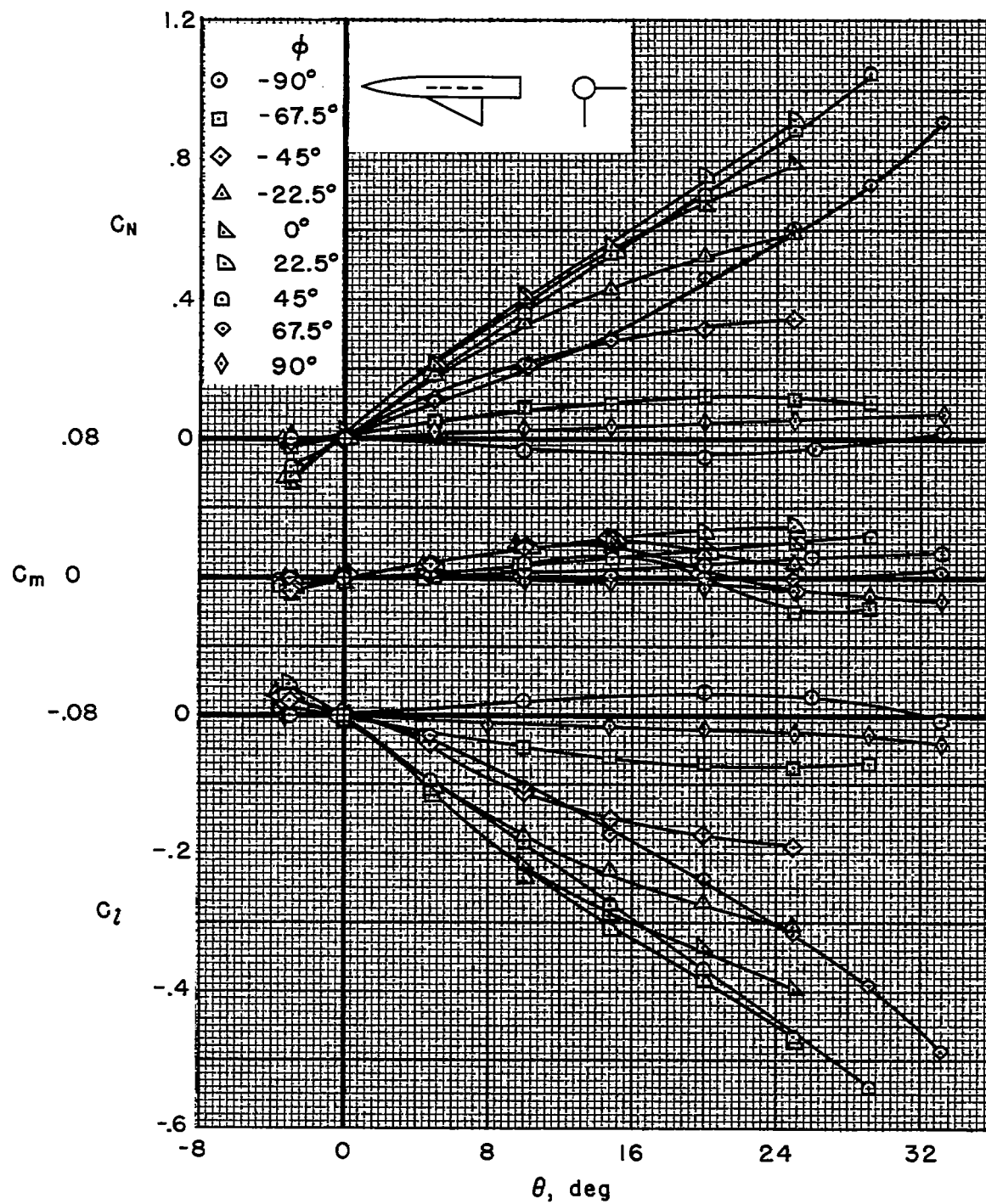
(d) $W_1(B_3W_2)$ configuration.

Figure 4.- Continued.

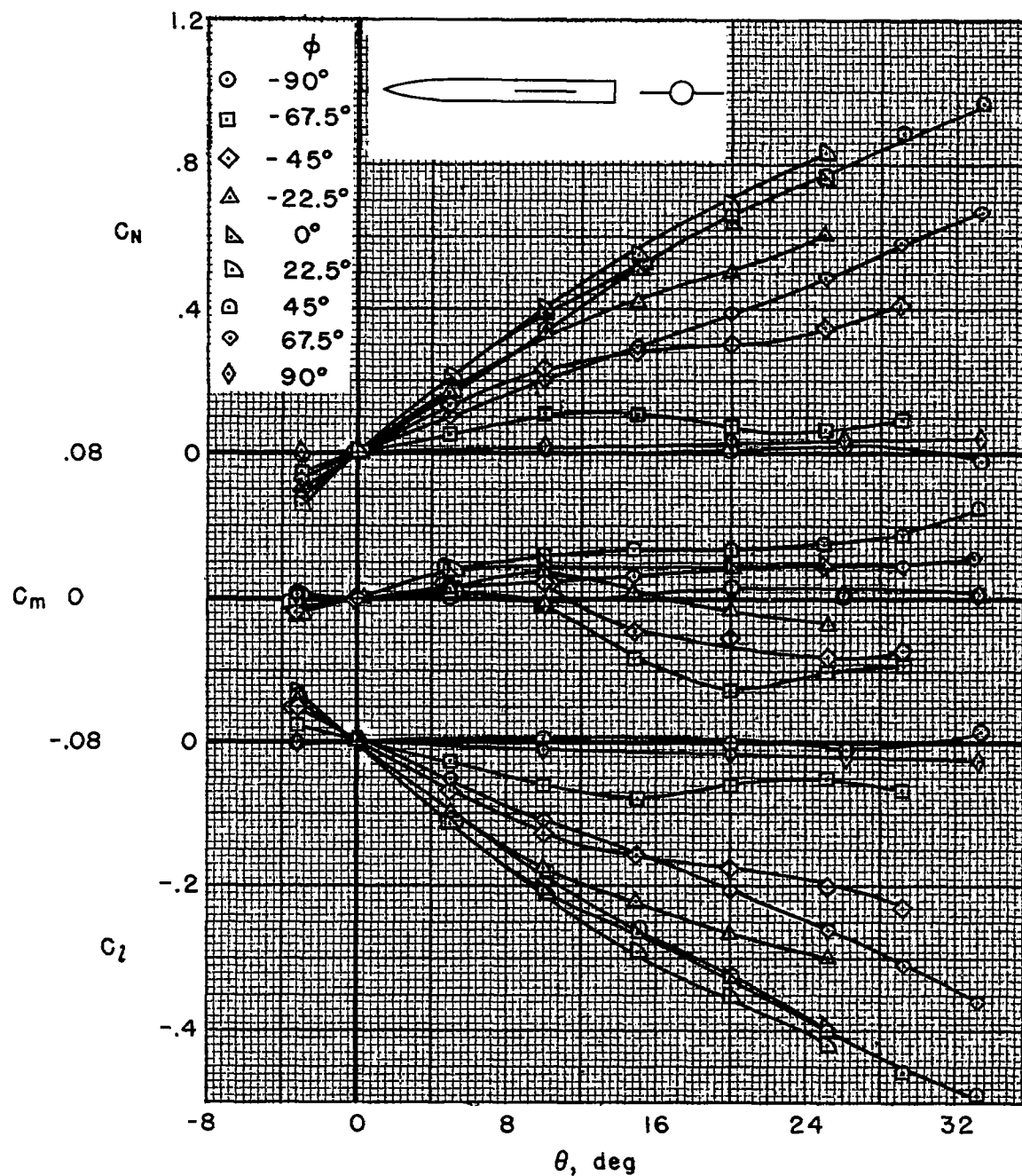
(e) $W_1(B_1W_3)$ configuration.

Figure 4.- Continued.

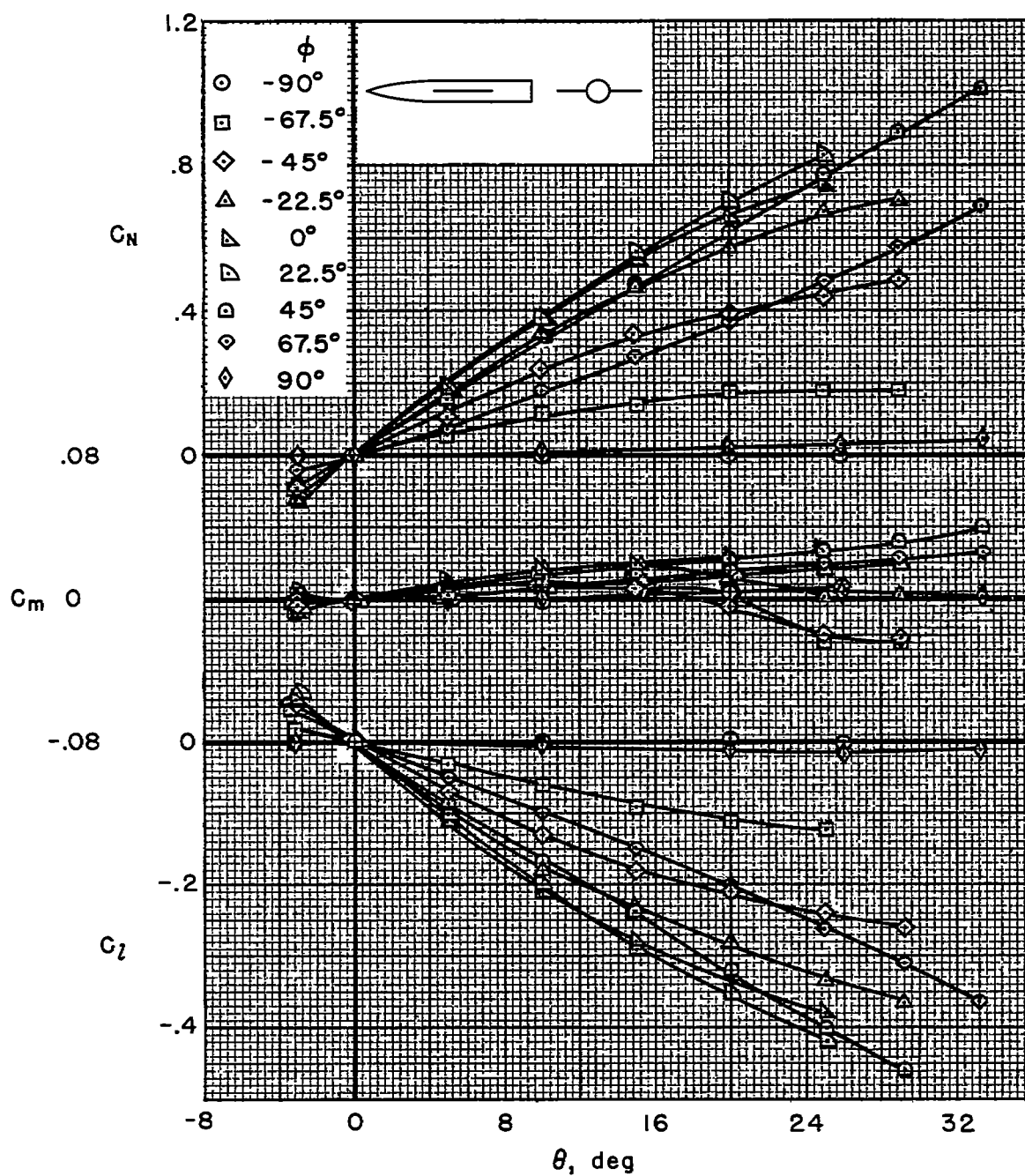
(f) $W_1(B_S W_3)$ configuration.

Figure 4.- Continued.

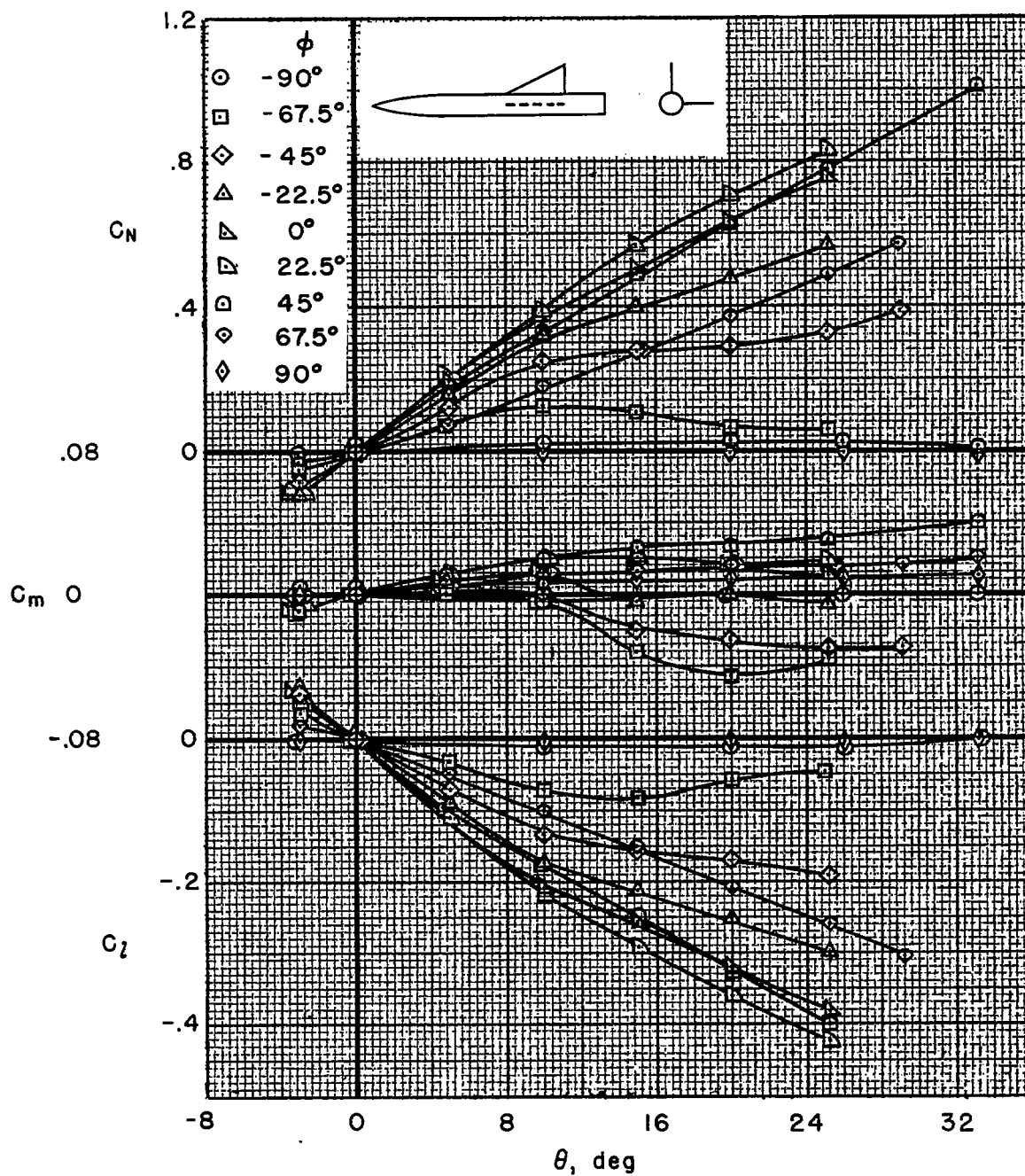
(g) $W_1(B_LW_4)$ configuration.

Figure 4.- Continued.

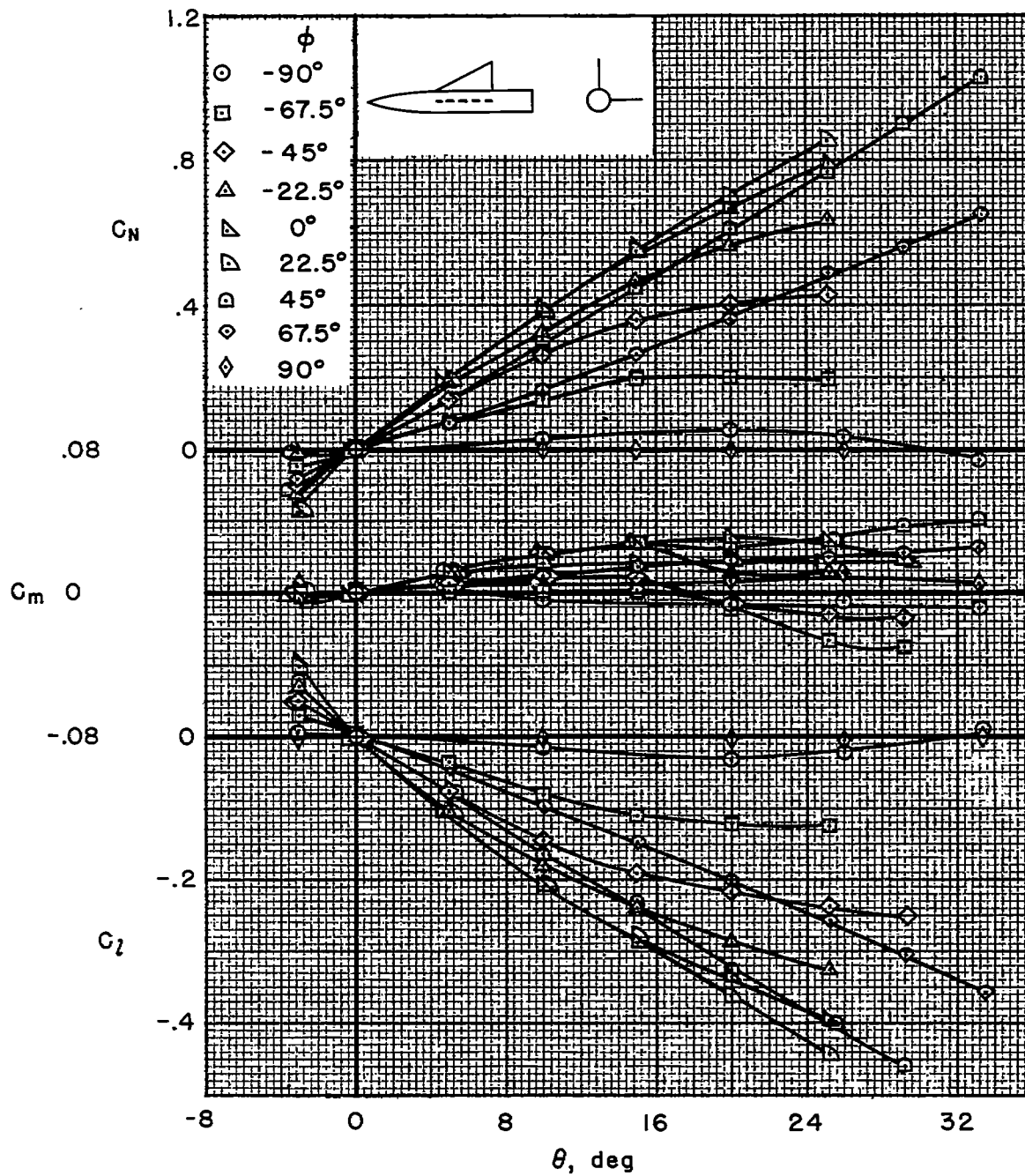
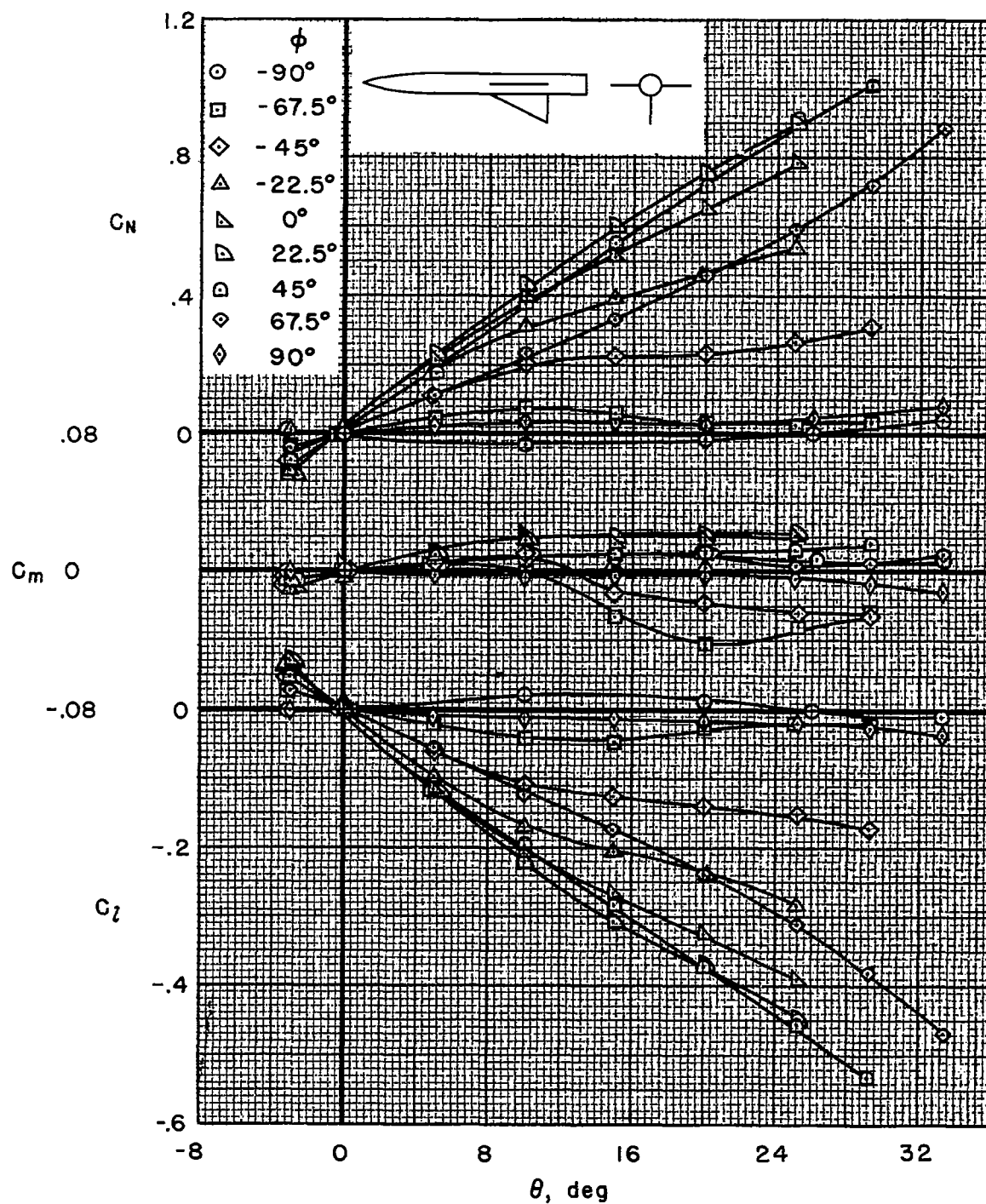
(h) $W_1(B_5W_4)$ configuration.

Figure 4.- Continued.



(1) $W_1(B_1W_2W_3)$ configuration.

Figure 4.- Continued.

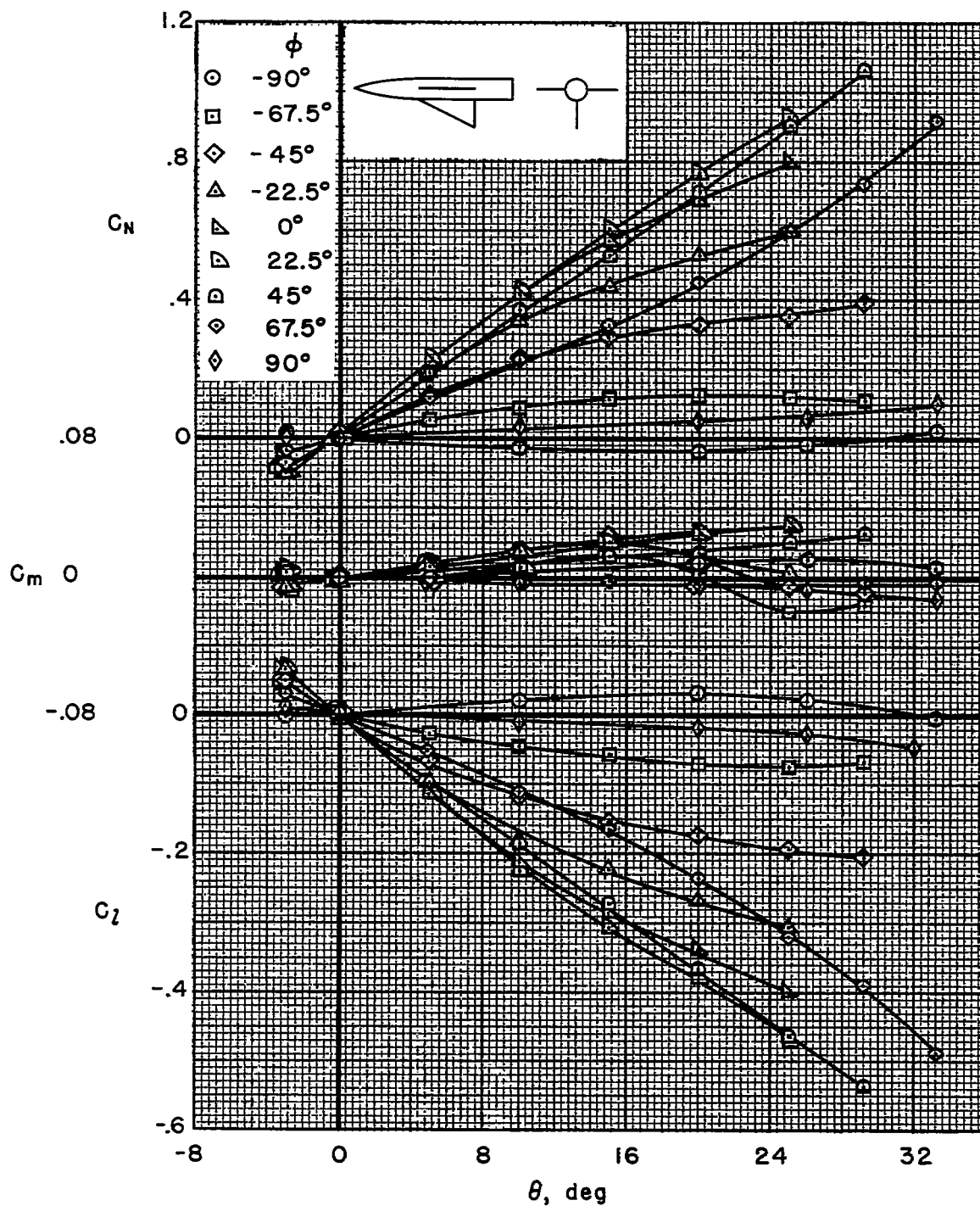
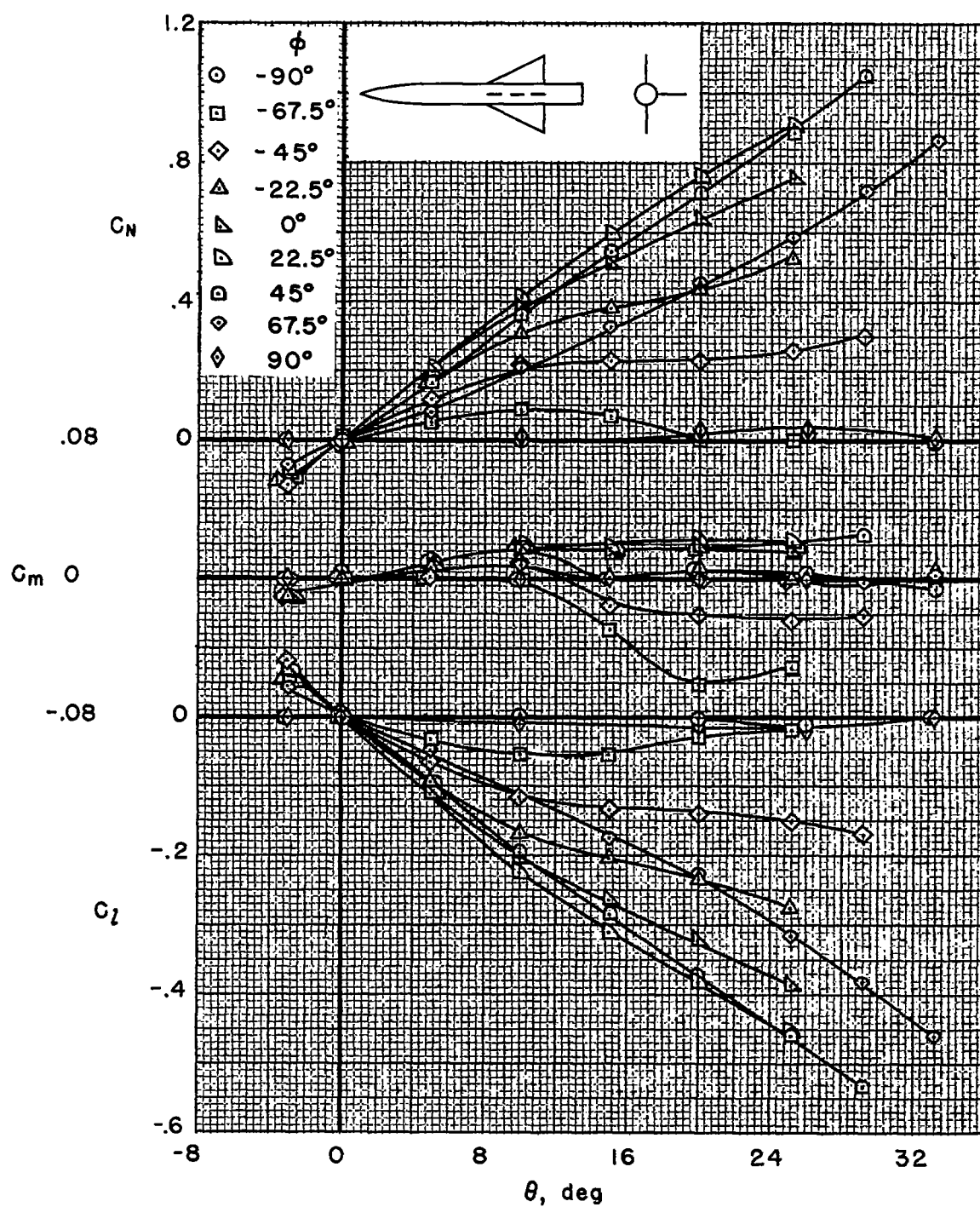
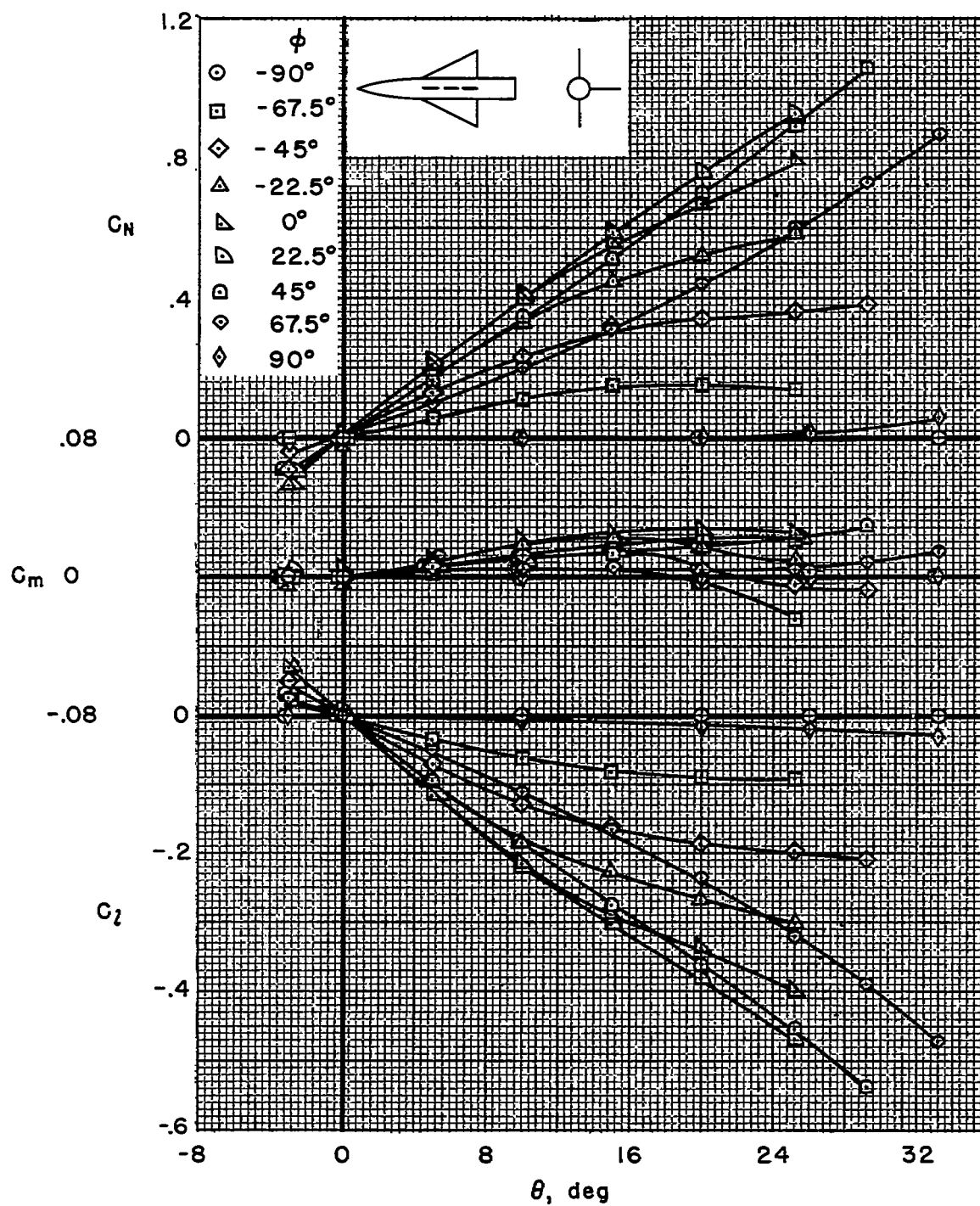
(j) $W_1(B_S W_2 W_3)$ configuration.

Figure 4.- Continued.



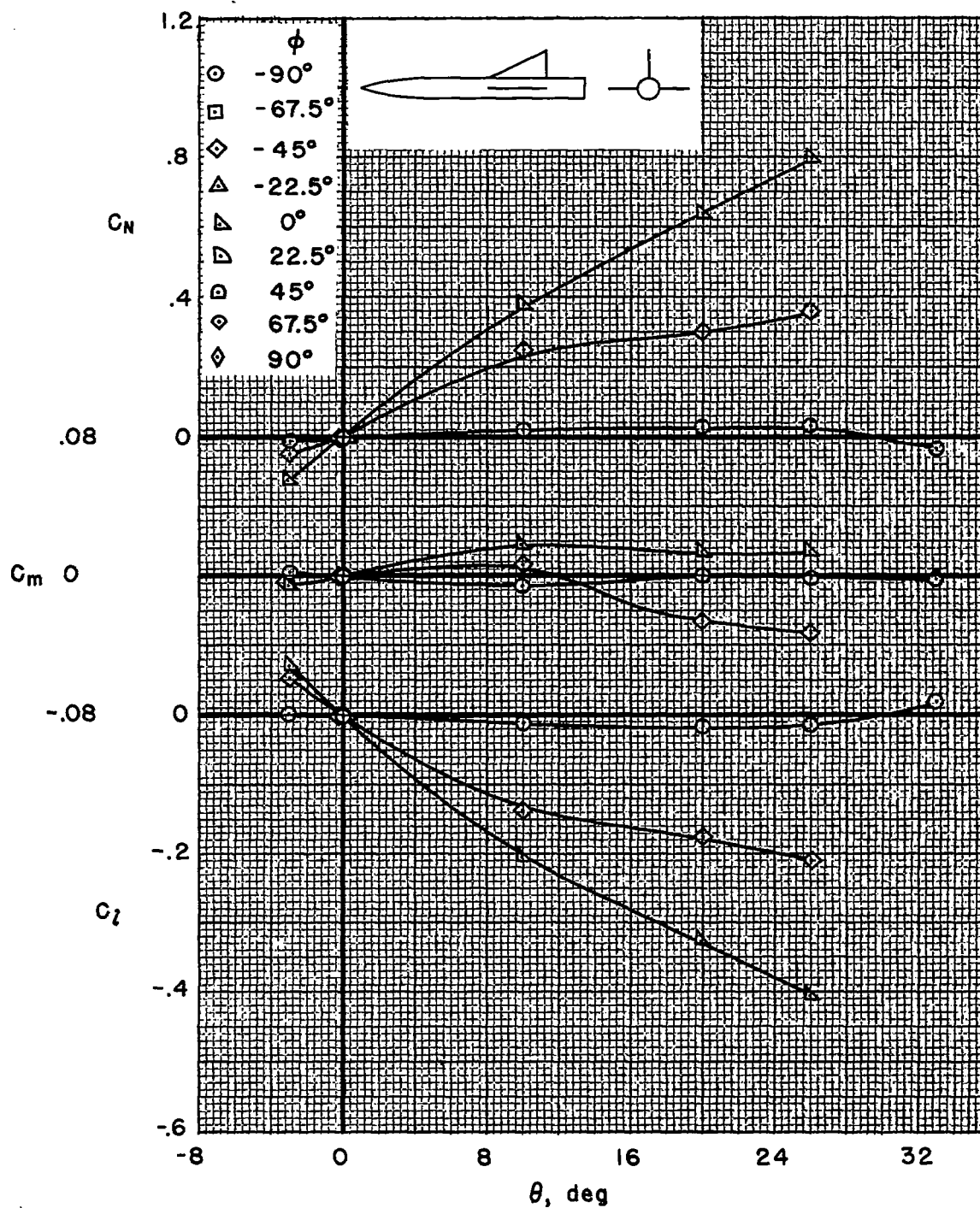
(k) $W_1(B_L W_2 W_4)$ configuration.

Figure 4.- Continued.



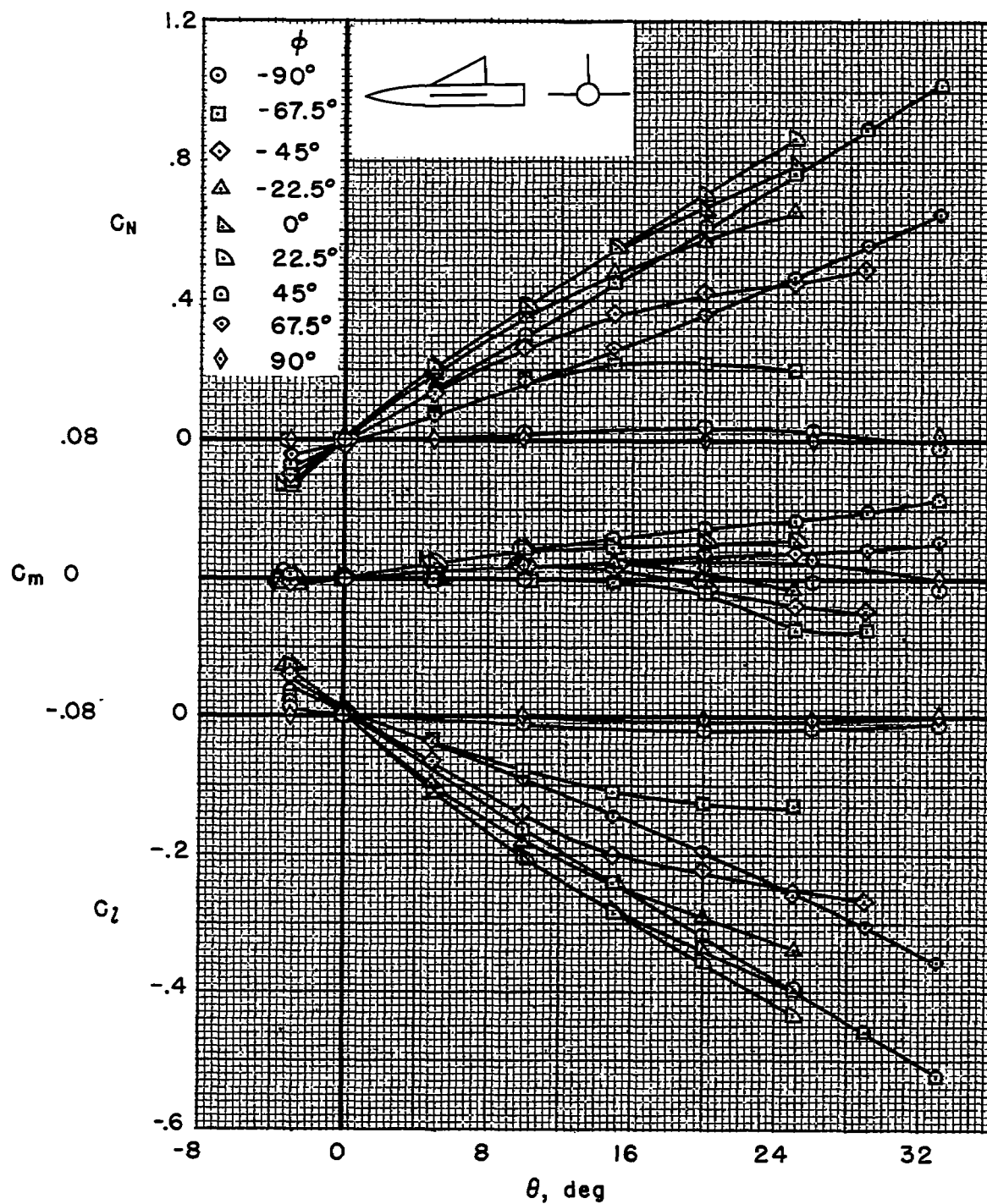
(1) $W_1(B_3W_2W_4)$ configuration.

Figure 4.- Continued.



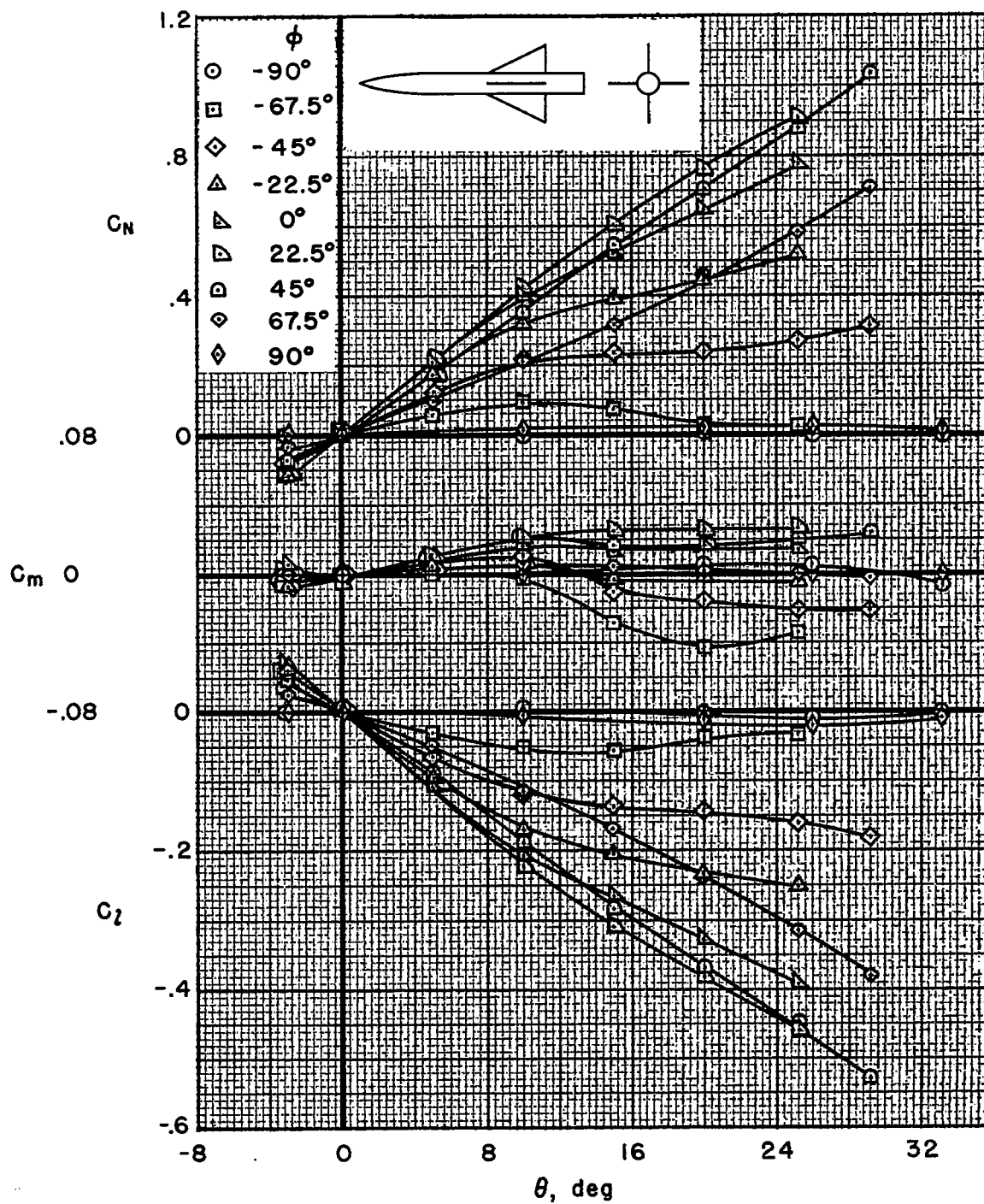
(m) $W_1(B_1W_3W_4)$ configuration.

Figure 4.- Continued.



(n) $W_1(B_S W_3 W_4)$ configuration.

Figure 4.- Continued.



(o) $W_1(B_L W_2 W_3 W_4)$ configuration.

Figure 4.- Continued.

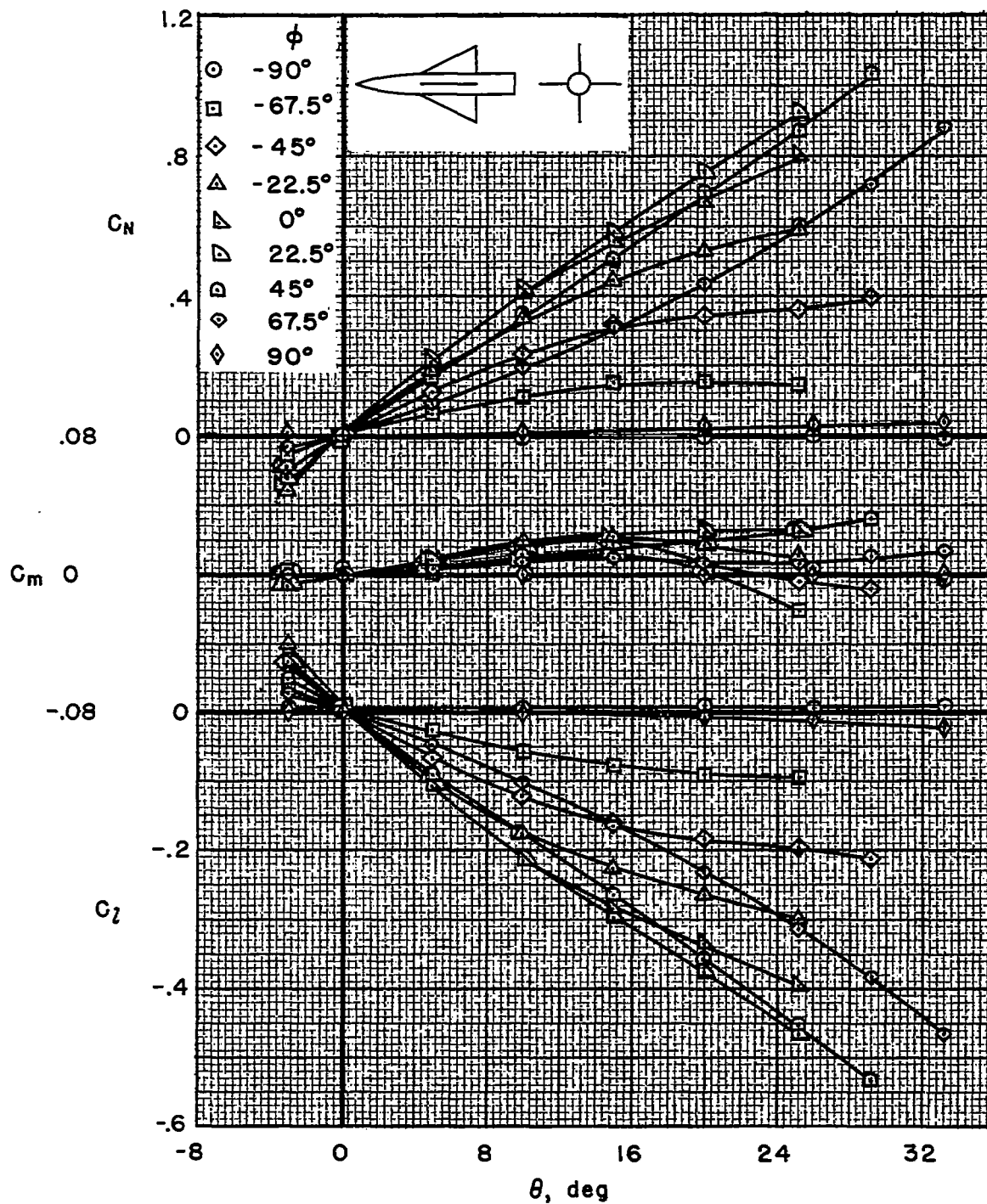
(p) $W_1(B_5W_2W_3W_4)$ configuration.

Figure 4.- Concluded.

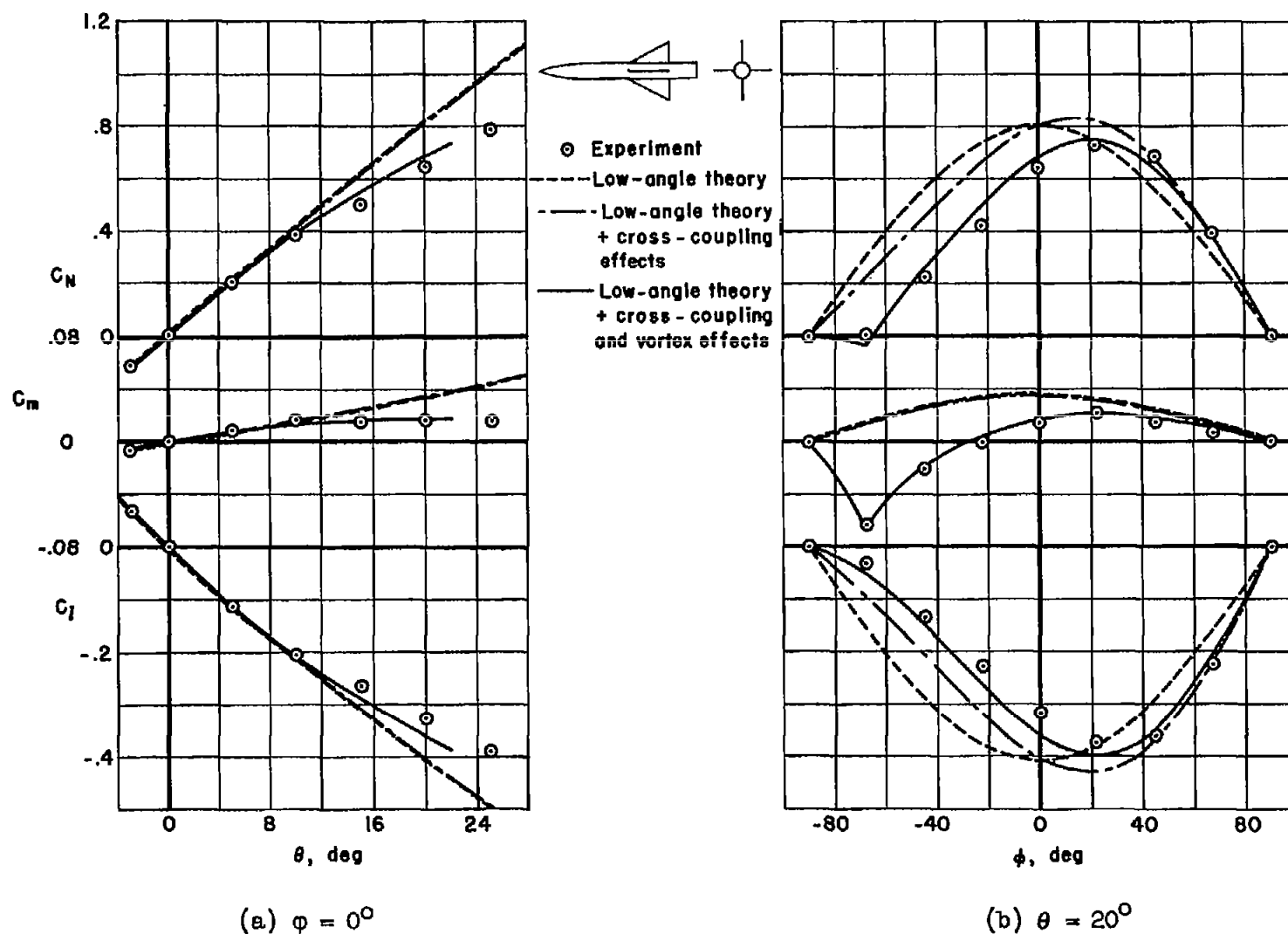


Figure 5.- Comparison of aerodynamic characteristics of wing panel W_1 with theory; $W_1(B_L W_2 W_3 W_4)$ configuration, $R = 1.03 \times 10^6$.

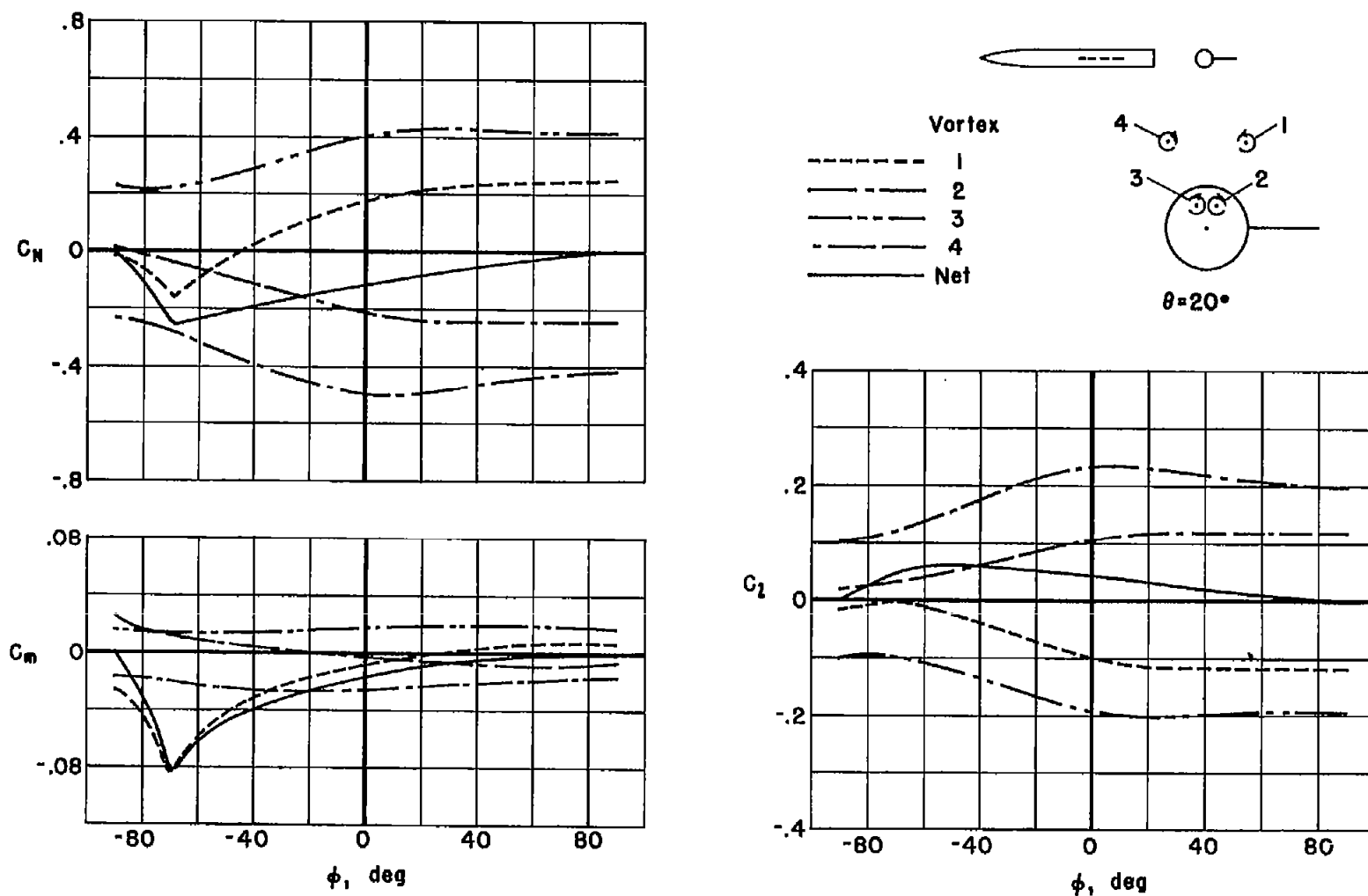


Figure 6.- Contribution of body crossflow vortices to calculated wing-panel characteristics at combined angles of pitch and roll; $W_1(B_L)$ configuration.

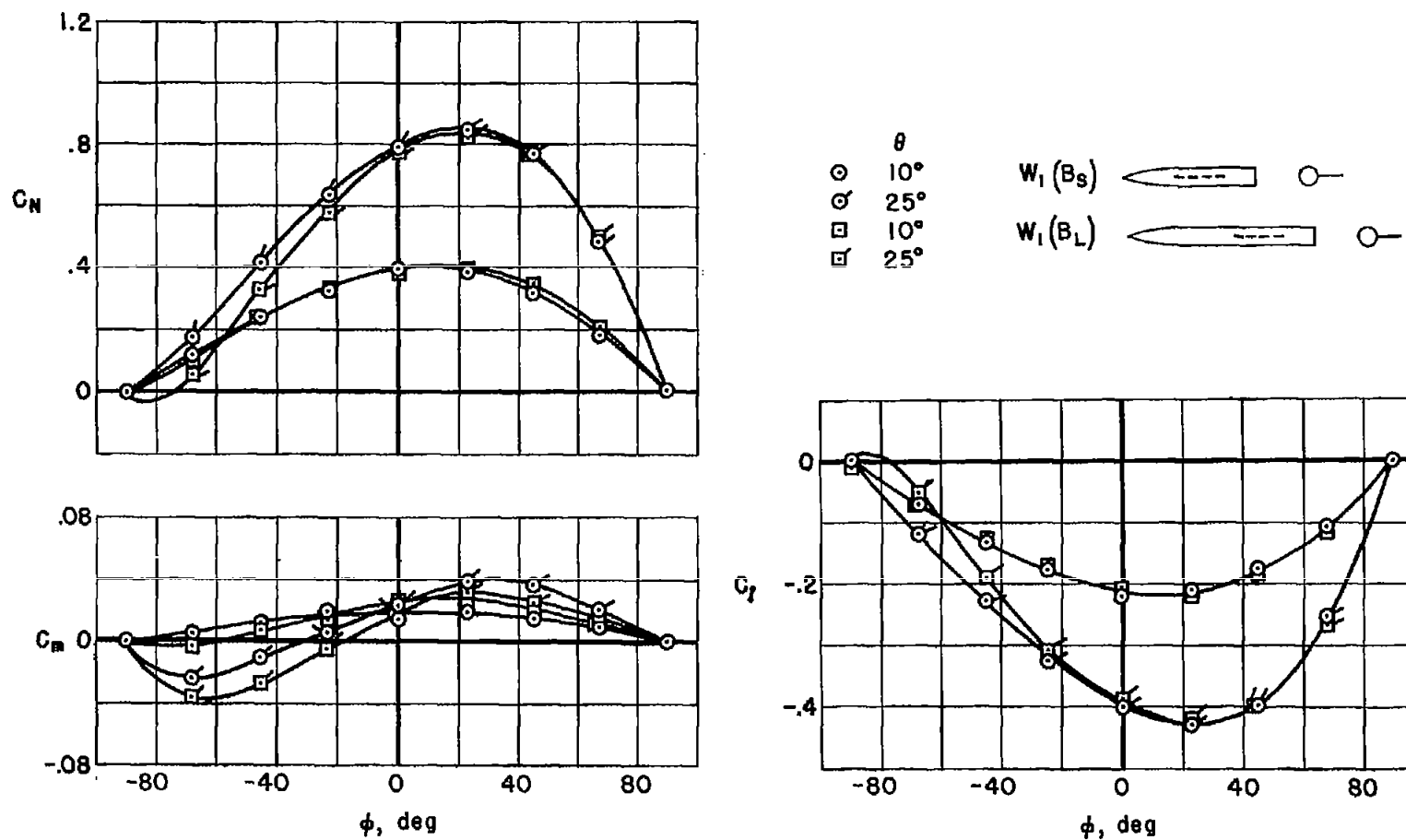
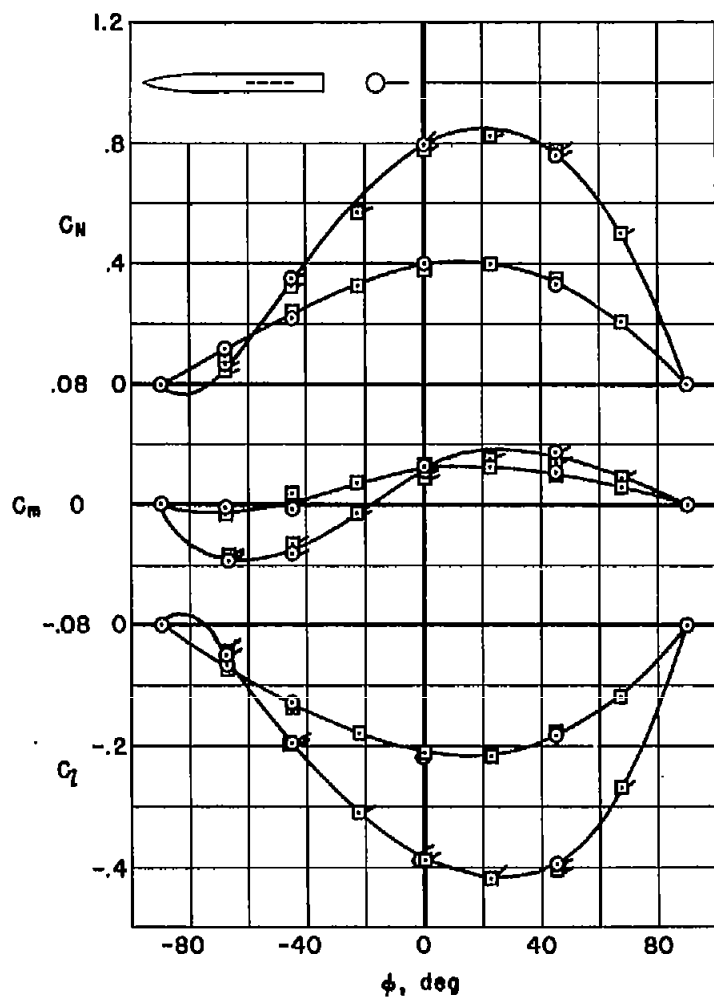
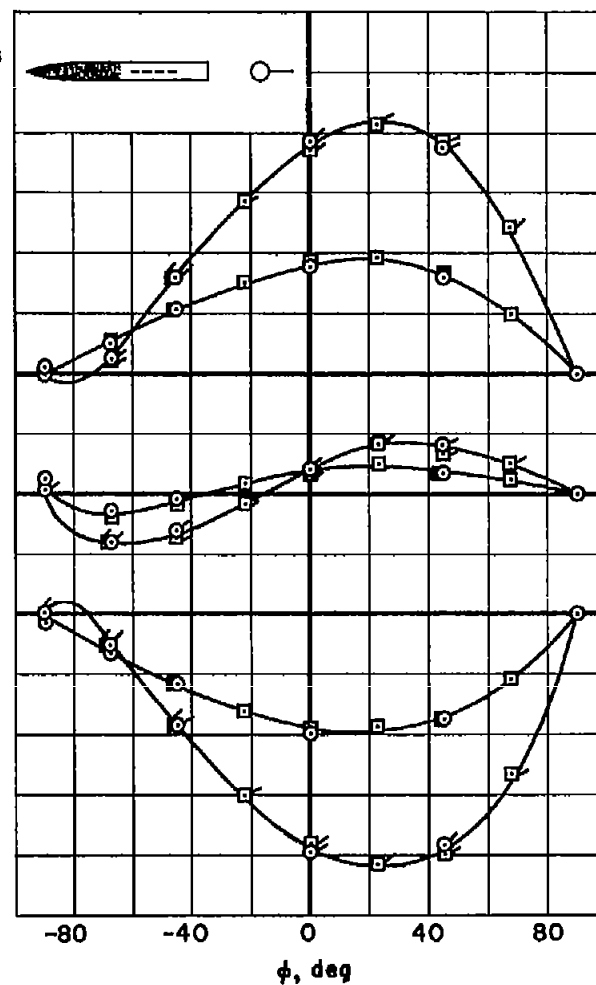


Figure 7.- Effect of forebody length on wing-panel characteristics.

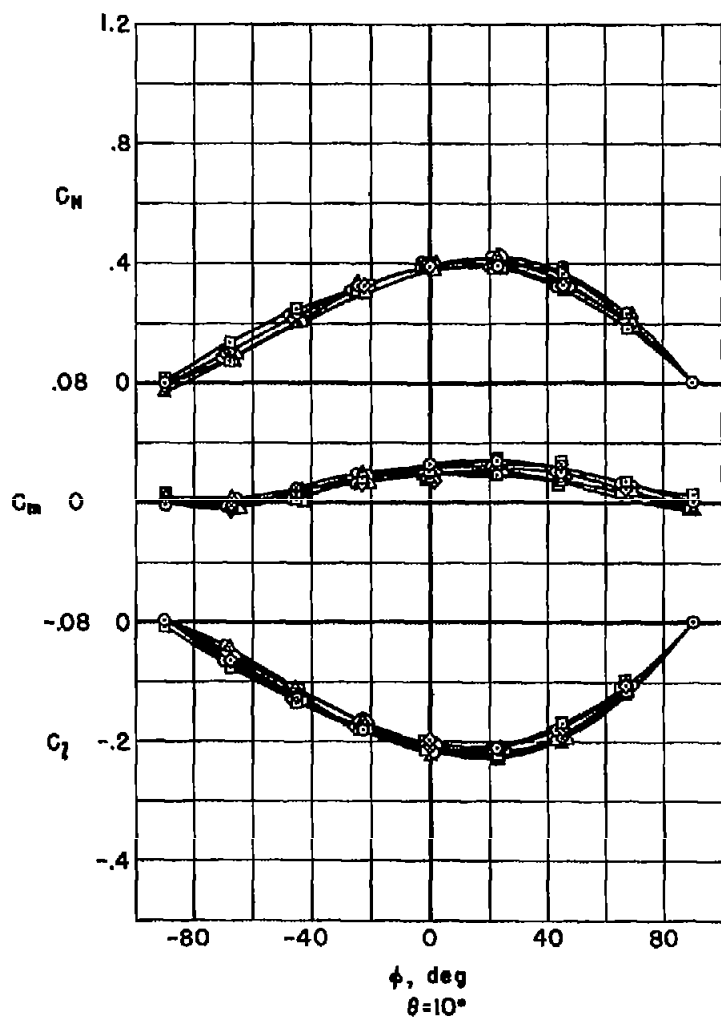


(a) Smooth forebody.



(b) Rough forebody.

Figure 8.- Effects of Reynolds number and forebody roughness on wing-panel characteristics; $W_1(B_L)$ configuration.



(a) Long forebody.

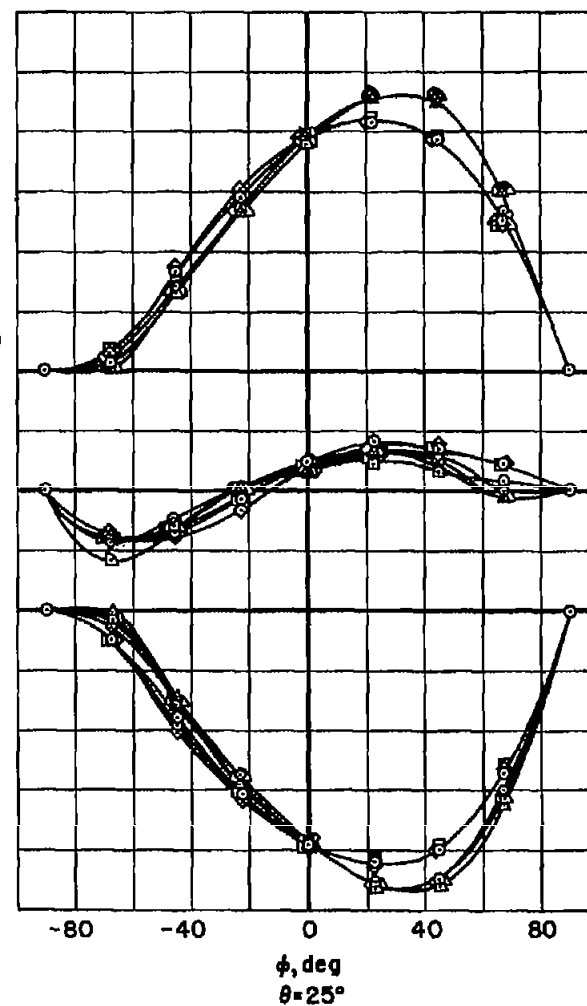
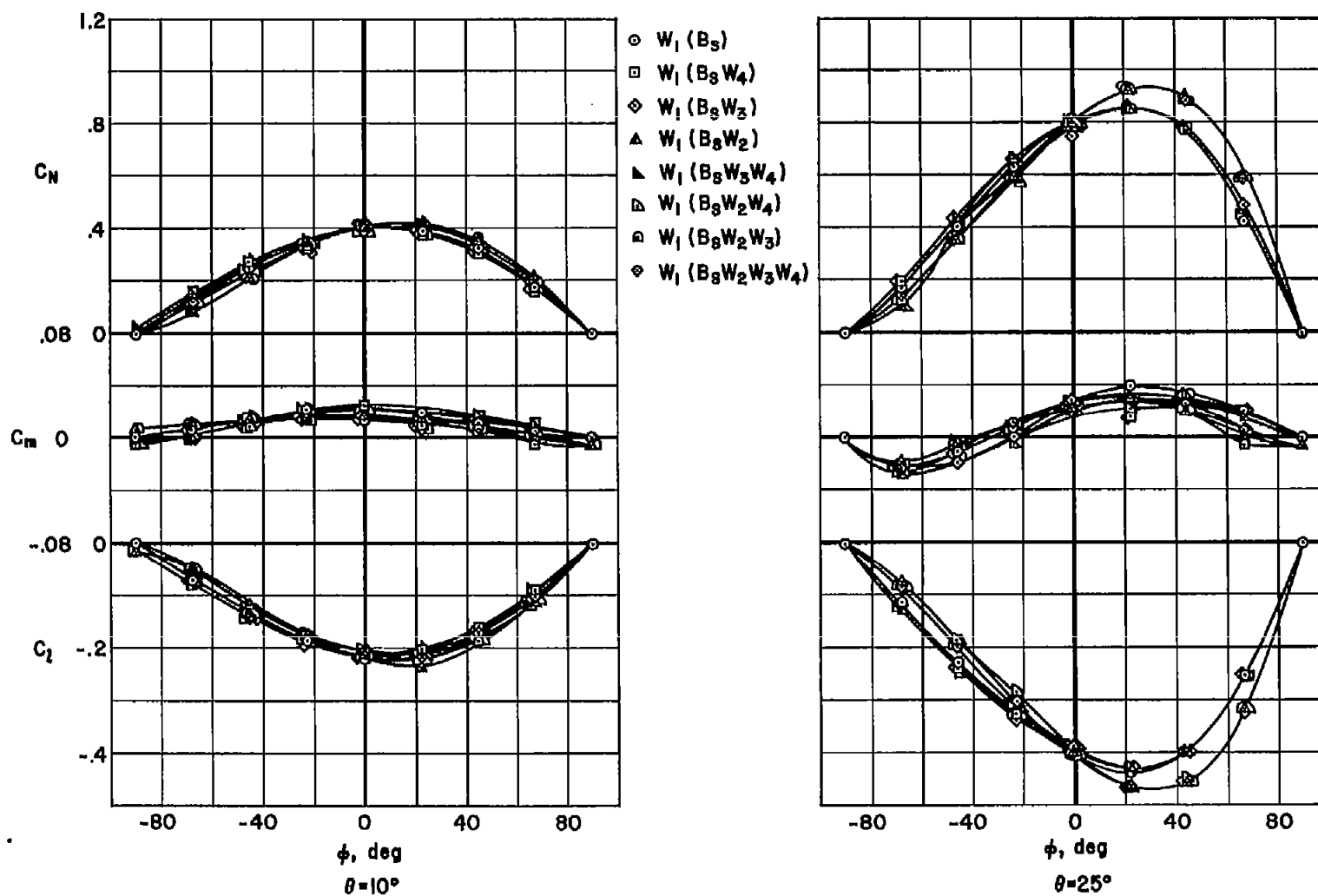
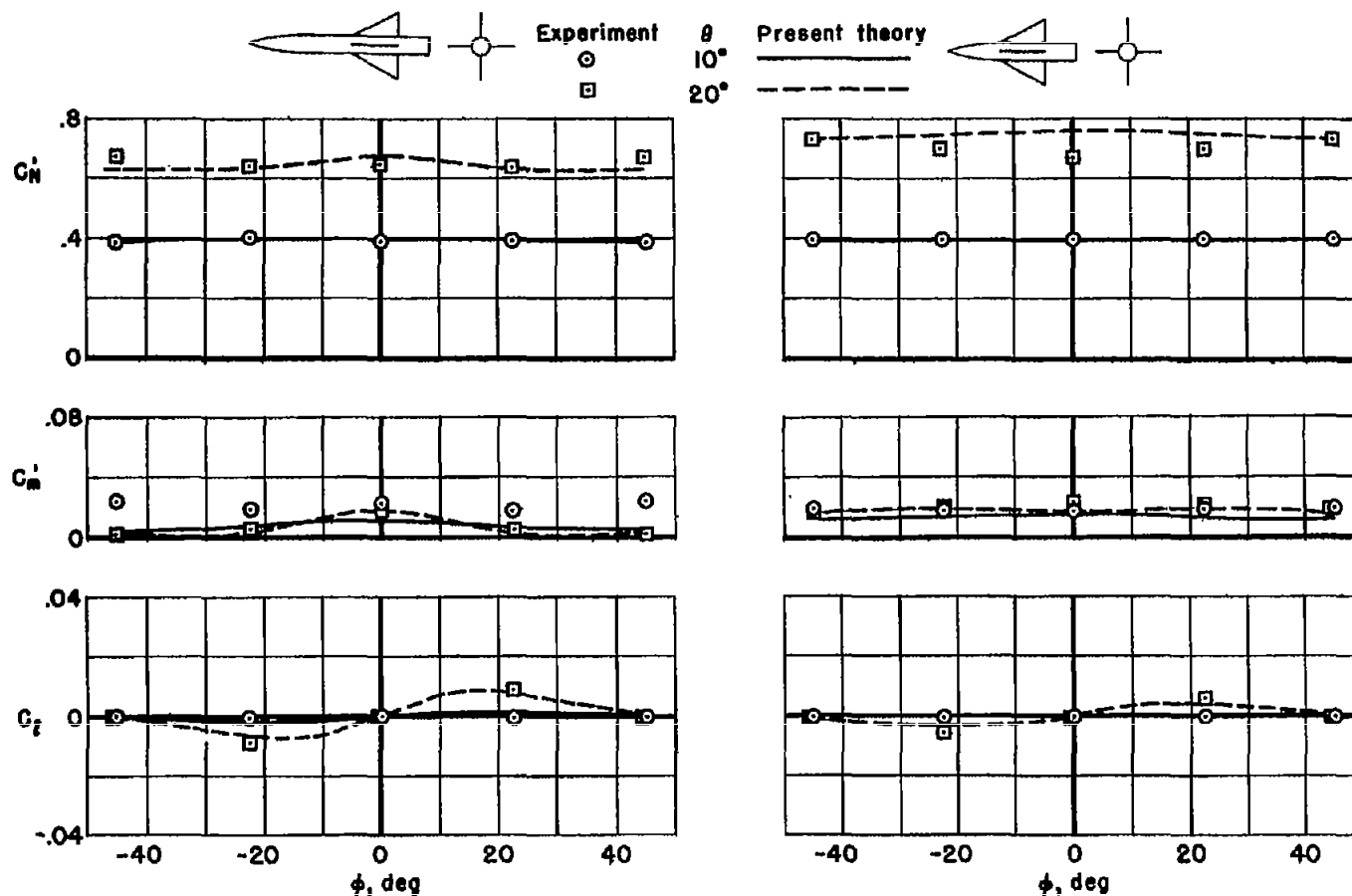


Figure 9.- Effects of panel-panel interference on wing-panel characteristics.



(b) Short forebody.

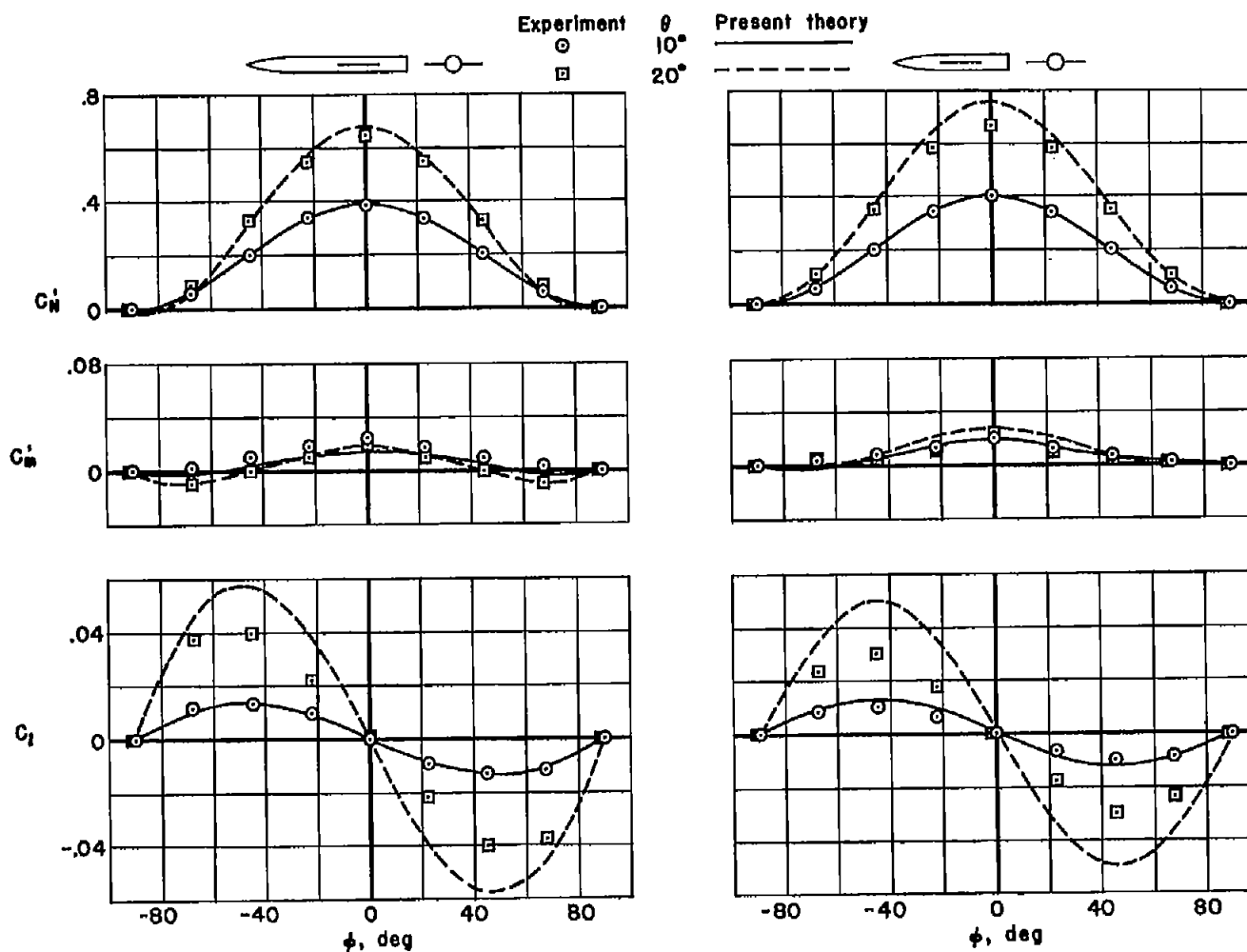
Figure 9.- Concluded.



(a) $W_1W_2W_3W_4(B_L)$ configuration.

(b) $W_1W_2W_3W_4(B_S)$ configuration.

Figure 10.- Aerodynamic characteristics of cruciform wing panels at combined angles of pitch and roll.



(a) $W_1W_3(B_L)$ configuration.

(b) $W_1W_3(B_S)$ configuration.

Figure 11.- Aerodynamic characteristics of planar wing panels at combined angles of pitch and roll.

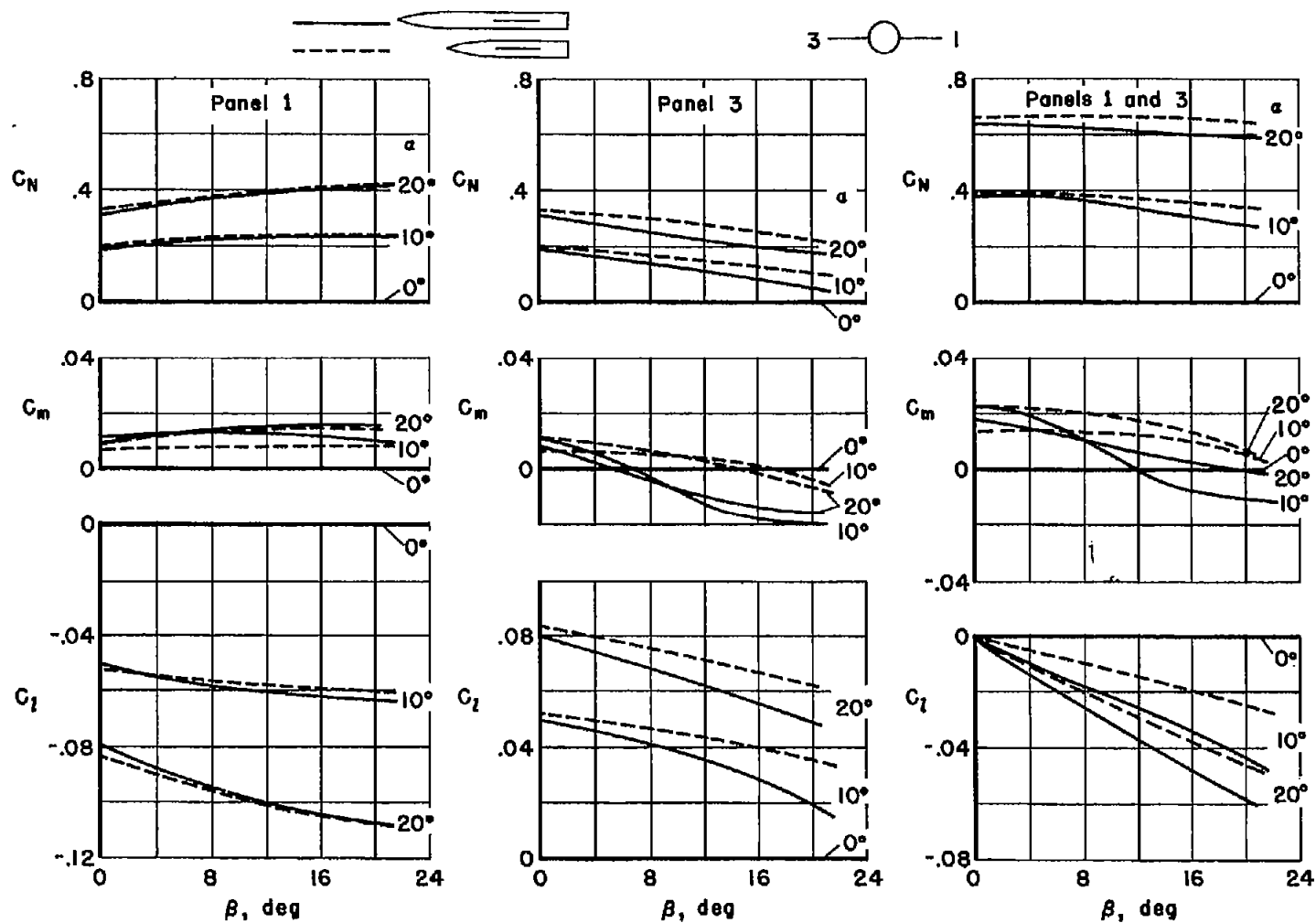


Figure 12.- Contribution of wing panels to aerodynamic characteristics of planar wing-body combinations at combined angles of attack and sideslip.

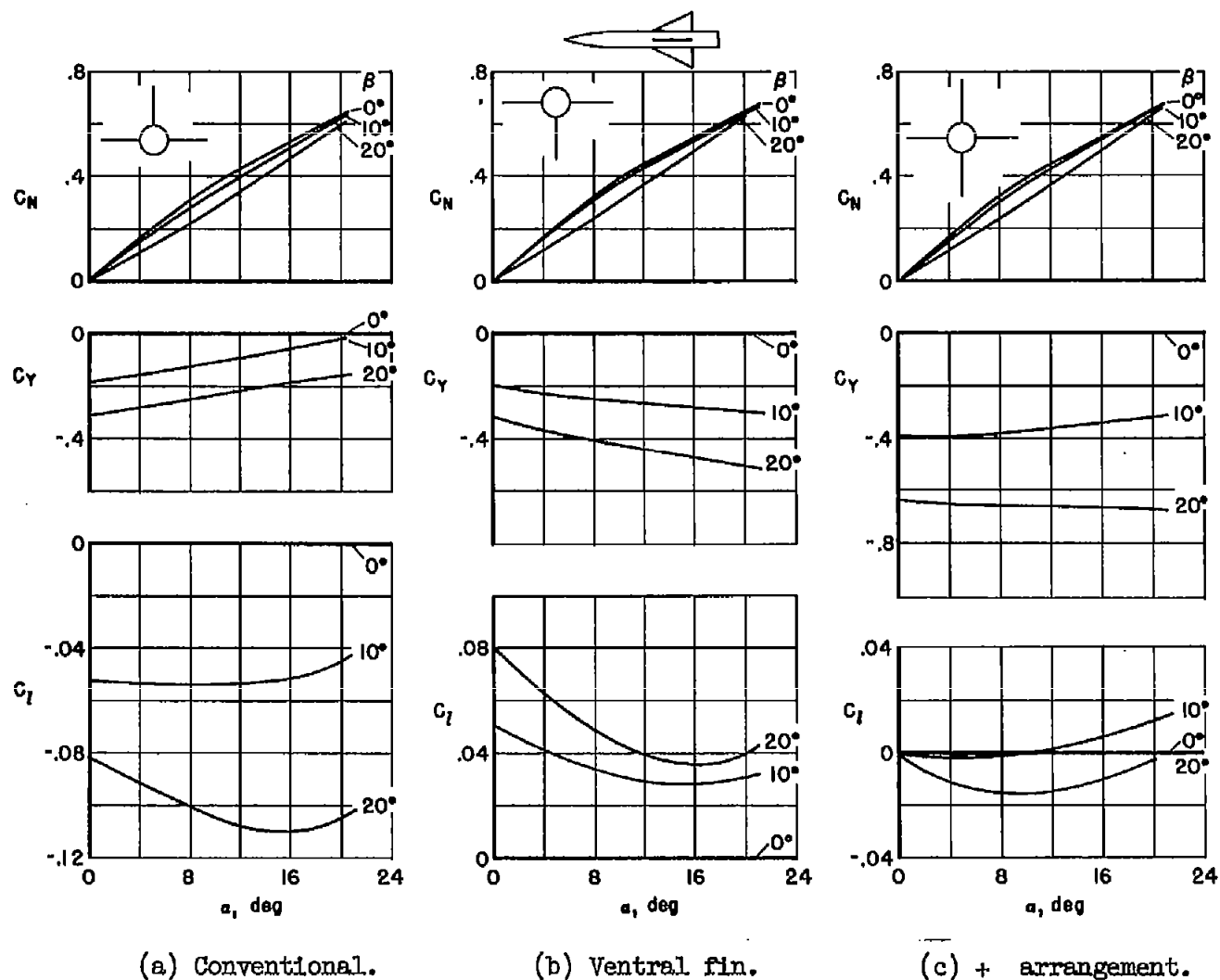
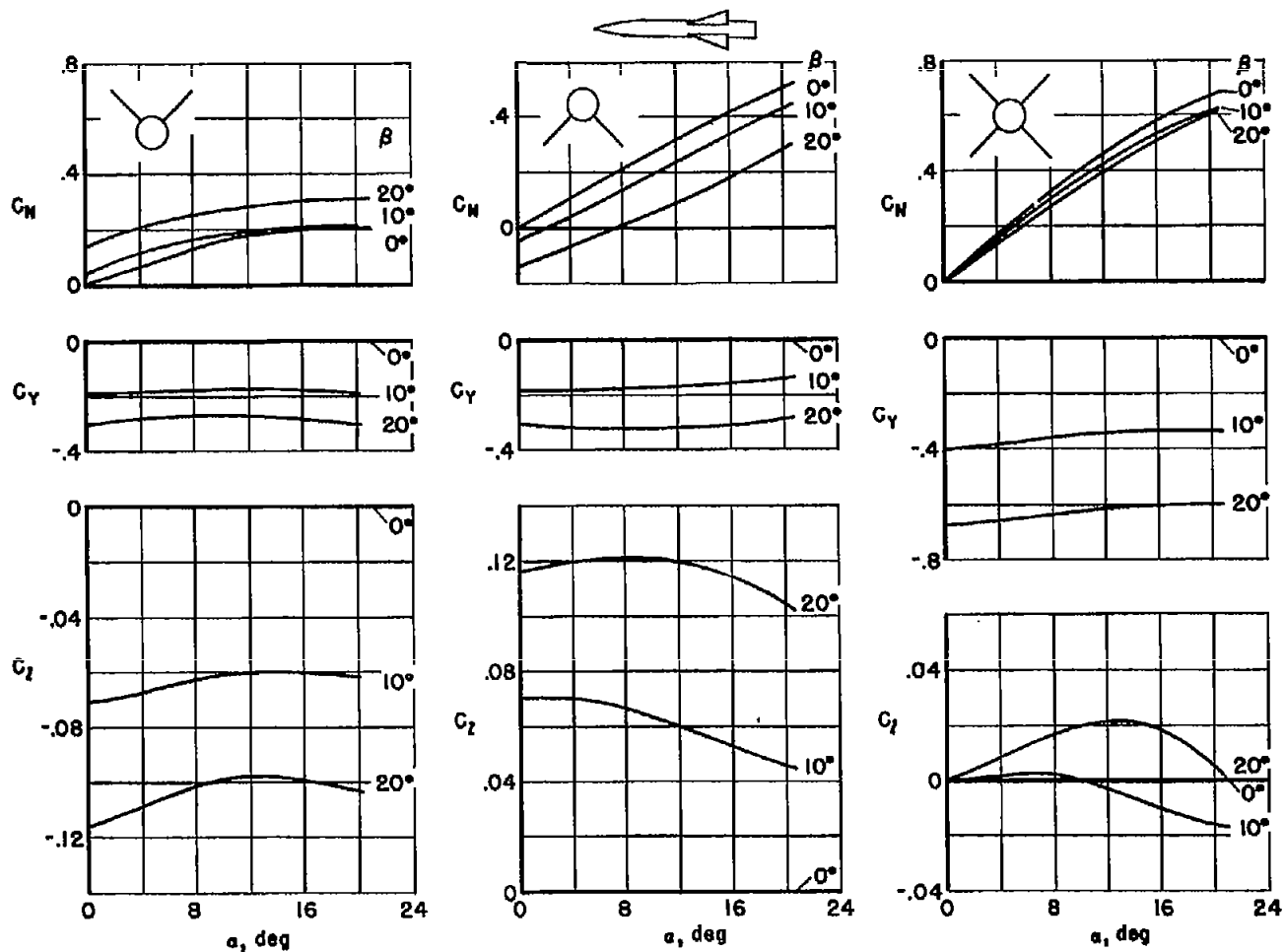


Figure 13.- Contribution of various tail-plane arrangements to longitudinal and lateral stability at combined angles of attack and sideslip; long forebody.



(d) V arrangement.

(e) Inverted V arrangement.

(f) X arrangement.

Figure 13.- Concluded.

2
3

4
5

6
7